Thesis

Ab Initio Calculations of Multiplet Terms for Rare Earth Ions

Shinichi Itoh

Department of Electronics Engineering,
University of Electro-Communications

December 13, 1993

Contents

Chapter 1

Introduction

Spectroscopic properties of rare earth ions in III-V semiconductors are one of the subjects of the absorbing interests for understanding electronic states of strongly correlated systems and opto-electronic device applications. In 1980, V. A. Kasatkin succeeded for the first time in observing the photoluminescence spectra of the doped rare earth ion, Yb, in GaP [1]. Since then, many researchers have devoted themselves producing a variety of rare-earth-doped semiconductors which show sharp luminescence spectra.

Rare earth ions as impurities are ionized to trivalent ions in semiconductors. Parts of the rare earth ions are considered to be the centers of the photoemissions. The photoemission spectra due to $4f$-$4f$ intra atomic transition are observed by many techniques, that is, photoluminescence (PL) [2, 3, 4, 5, 6, 7], cathode-ray luminescence [8], and electroluminescence (EL) experiments [9, 10, 11]. In luminescence experiments, rare earth ions in semiconductors provide deep impurity levels in the energy gap of the host materials. The electronic structure of rare earth ions in semiconductors is one of the attractive problems in semiconductor physics. It is necessary to develop a theoretical approach for systematic analysis the luminescence spectra.

The $4f$ orbitals of a rare earth atom are screened by the outer occupied orbitals, $5s$ and $5p$. Even when a rare earth atom is ionized to a trivalent ion in III-V semiconductors, the $4f$ orbitals are very weakly affected by the crystal field. Thus the shape of the $4f$ related photoluminescence spectrum is very sharp, reflecting the atomic nature. In fact, the wavelength of the peak intensity does not depend much on the kinds of host semiconductors [12].

Since the $4f$ orbitals are of partially occupied open-shell structure, the complicated multiplet terms of $4f$ electrons are formed. That is, strong Coulomb interactions ($\sim$ 10 eV) between $4f$ electrons produce the multiplet terms denoted by ${}^{2S+1}L$, as is known Russell-Saunders coupling. Here L and S are the total orbital and spin angular momenta, respectively. Further, spin-orbit (SO) interactions ($\sim$1 eV) split the multiplet terms into some levels denoted by ${}^{2S+1}L_J$, in which only the total angular momentum J preserves in the presence of SO interaction. Furthermore, the multiplet terms denoted with ${}^{2S+1}L_J$ are splitted into fine structures by the crystal field due to ligand semiconductor atoms ($\sim$ 0.1 eV). Thus the hierarchic interactions are working on the $4f$ electrons in the system.

In order to explain the electronic structure of $4f$ electrons, some theoretical approaches have been proposed for a rare earth atom and a cluster. Among them, the DV-Xα is one of the useful theoretical method for the analysis of one-electronic structures of clusters[13]. The calculated results can be applied to x-ray photoemission spectra (XPS) [14, 15]. The XPS spectra corresponding to the transitions of $4f$ electrons are assigned to the energy gaps between the one-electron orbital energies [14, 15]. But the picture of one-electron states cannot be applied to the present problem of the photoluminescence spectra of rare earth ions because the sharp PL spectra comes from the intra-excitations in the multi-electronic structures of $4f$ electrons. The essential character of luminescence spectra is relevant to the existence of the multiplet structures which result from the open-shell configurations of $4f$ electrons. Since the $4f$ orbitals are localized in semiconductors, the multiplet structures are effective even in the semiconductors.

The purpose of the present thesis is (1) to develop an *ab initio* calculation of the multiplet terms for $4f$ electrons, (2) to investigate hierarchic interactions of Coulomb repulsion, SO interaction and crystal field effect for rare earth ions in semiconductors and (3) to clarify the mechanism of luminescence.

Experimentally, four rare earth ions, Yb^{3+}, Er^{3+}, Nd^{3+} and Tm^{3+} in semiconductors have been intensively investigated. Among these ions, the Er^{3+} ion in III-V semiconductors is known to show a strong and sharp photoluminescence whose peak wavelength (1.54μm) corresponds to that of the minimum energy loss in optical fiber cables. As for host III-V semiconductors, InP, GaAs and GaP are commonly used by many researchers. Trivalent atoms in the III-V semiconductors are substituted with trivalent lanthanide ions. There are some methods to produce rare-earth-ion-doped semiconductors, i.e. diffusion [16, 17], liquid phase epitaxy (LPE) [2, 4, 18], ion implantation [3, 7, 19, 20], metal organic chemical vapor deposition (MOCVD) [2, 21, 22, 23] and molecular beam epitaxy (MBE) [6, 24]. Among a variety of combinations of rare earth ions and host semiconductors, Yb incorporated in

InP has been extensively investigated because the multiplet structure of Yb is simple and the intensity of the luminescence is relatively strong. The ESR experiments shows that the position of Yb^{3+} doped in the crystal InP is in place of In^{3+} [5, 20].

In order to explain the photoemission spectra of $4f$ electrons, a theoretical approach by perturbation approximation has been successfully performed by Judd and Ofelt in 1960's [25, 26]. Since SO interaction and crystal field effects are relatively small compared with Coulomb interactions, these effects can be treated as a perturbation in an effective Hamiltonian with use of adjustable parameters. The calculated results are fitted to the optical spectra. The Judd-Ofelt theory has extensively been applied to spectrum analyses of optical measurements for chemical trends of rare earth ions in ionic crystal $LaCl_3$. In their theory the multi-configurations for $4f$ electrons include the excitations to $5d$ and $6s$ orbitals. Further, the intermediate coupling of spin-orbit interactions is much effective for multiplets of rare earth ions. This effect is included in the second order perturbation. The enormously large number of observed multiplet terms could be fitted to the multi-electronic excited states in the region $\sim 50{,}000\ \mathrm{cm}^{-1}$ by considering these excitations. However, the various parameters are empirically determined so as to reproduce the multiplet energies, i.e. spin-orbit constants, coefficients of perturbed wave functions between $4f$ and its outer orbitals, crystal field parameters and so on. Thus it is difficult to explain the physical meaning of the obtained parameters from the microscopic theory for the electronic structure, and this method can not be applied to unknown materials.

With a rapid progress on computational and theoretical methods, non-empirical approaches of computational physics and chemistry have been developed. Hemstreet calculated the one-electron energy levels of Yb^{3+} in InP by the relativistic DV-Xα cluster calculation [27]. The paper discussed the relationship between the charge distribution and the $4f$ energy levels of Yb^{3+}. The calculated results show that the ionicity of an Yb ion in InP is between Yb^{2+} ($4f^{14}$) and Yb^{3+} ($4f^{13}$) in the ground state. Although the total amount of charge in the $4f$-shell increases from 13.60 to 13.80 upon ionization, the total electronic charge of Yb impurity changes only 68.90 to 68.93. (It is noted here that the atomic number of Yb is 70.) This fact indicates that the valence electrons of the host redistribute themselves away from the impurity so as to retain local charge "neutrality" of the impurity Yb. In this way, the DV-Xα method has shown that the interactions between the $4f$ electrons and the valence electrons are not negligible.

So far the *ab initio* calculation for obtaining the multiplets of the $4f$ electron systems have not been performed until recently [28]. Especially, spin-orbit (SO) interactions for $4f$ electrons and the crystal field effects have not been taken into account simultaneously in *ab initio* calculations of clusters. As for atomic calculations, SO splitting can be obtained by numerical Hartree-Fock equations and the calculated results are tabulated in the literatures [29]. But it is difficult to apply this method to clusters containing heavy atoms since it is beyond the limitations of computations with the numerical basis sets. In an *ab initio* calculation, Gaussian basis sets are widely used for the practical reason that the integrations of electron-electron interactions can be obtained analytically.

In the present thesis, we calculated multiplet terms of the strongly correlated $4f$ electrons of trivalent lanthanide ions taking into consideration SO interaction and weak covalent crystal field effect. We especially investigate the role of the contracted Gaussian basis functions of $4f$ orbitals on a first principle calculation. In order to calculate the multiplet terms of rare earth ions doped in crystals semiconductors, SO configuration interaction (SOCI) calculations have been performed for the six lanthanide ions, Pr^{3+}, Pm^{3+}, Eu^{3+}, Tb^{3+}, Ho^{3+}, Tm^{3+} and a $(\mathrm{TmP}_4)^{3+}$ cluster. In the SCF and CI calculations for the six ions, we investigate the relationship between the contractions of the Gaussian basis sets and the obtained multiplet energies. And we present suitable contractions of the $4f$ basis functions. Since a selection of Gaussian basis sets is one of the most important problem in a *ab initio* method, the present picture of the contractions of the $4f$ radial functions is meaningful. We will show that the results of the SOCI calculations with use of our Gaussian basis sets reproduce the multiplet energies observed in the experiments.

Recently the $4f$-related PL spectra of Tm^{3+} ions in InP have been observed [12]. The wavelength of the peak of $4f$-$4f$ transition is 1.23 μm ($\sim 8100\ \mathrm{cm}^{-1}$) which is assigned to the transition of the multiplets, ${}^3H_5 \to {}^3H_6$. The shape of the spectrum is sharp, showing that the Tm^{3+} portion has a sufficiently atomic nature even in InP. However, the crystal field effect can not be neglected as it lowers the spatial symmetries of the $4f$ electrons. Tm^{3+} is located at the tetrahedral site surrounded by four P atoms, assuming that Tm^{3+} is substituted for In^{3+}. The spatial symmetry of the $4f$ electrons is the tetrahedral point group, T_d. We include the crystal field in a $(\mathrm{TmP}_4)^{3+}$ cluster. Main results of the tetrahedral crystal field effect on the SO multiplet levels of $4f$ electrons is presented in this thesis.

Finally, let us discuss the relativistic effect of rare earth ions. The relativistic effect is important for the inner core electrons of heavy rare earth ions since the kinetic energy of a core electron is close to the rest energy of an electron. The relativistic effect is included in so-called effective nuclear charge in the spin-orbit Hamiltonian for $4f$ electrons of the trivalent lanthanide ions. The effective nuclear charges were used as adjustable parameters for reproducing experimentally observed spin-orbit splittings. In the present thesis, we propose the non-empirical method for calculating effective nuclear charges for the first time by solving atomic Dirac-Slater equations. We will show that the present method for obtaining the effective nuclear charges is consistent with the spin-orbit CI calculations for the $4f$ electrons.

In the computations, we use library programs 'COLMBS' at Computer Center, Institute for Molecular Science, Japan. The original COLUMBUS [30] are modified to introduce the SO interactions in the spin-dependent unitary group direct CI algorithm [31]. Further we incorporate open-shell energy coefficients which are suitable for the present purpose. In the *ab initio* method we can perform CI calculations with considering SO and crystal field effects simultaneously. It is stressed that the library, COLMBS, is applied for the first time to the SOCI calculations of $4f$ electrons in the present thesis and that many modifications of COLMBS have been done for the application to $4f$ electrons in the collaboration with Satoshi Yabushita.

The organization of the thesis is as follows. In chapter 2, we review the backgrounds for the present thesis. In chapter 3, the methods of calculation are presented. The procedures of SCF and SOCI calculation are explained. In order to investigate the SO formula adopted in *ab initio* calculations more precisely, we calculate the effective nuclear charge for $4f$ electrons of rare earth ions by solving Dirac-Slater equation. In chapter 4, the calculated results for the multiplets of some trivalent ions and a cluster are shown. We discuss the relationship between effective nuclear charge and multiplet energies. Finally, in chapter 5, conclusions for the present thesis are given.

Chapter 2

Backgrounds

In this chapter, we briefly review the history of work on the luminescence of rare earth ions. The basic terminology and main results of experiments are reviewed in 2.1. Reviews of other work on *ab initio* calculations for f electrons are given in 2.2.

2.1 Luminescence spectra of rare earth ions

2.1.1 Basic theory of multiplet terms

In this section, we summarize the basic theory of calculating multiplet structures of rare earth ions. Further we explain the luminescence spectra quantitatively with use of the terminology.

The $4f$ orbitals have the angular momentum $l = 3$ in the spherical symmetric potentials and they are degenerated without any other interactions on the $4f$ electrons. The $4f$ orbitals consist of seven orbitals which can be specified by the z-components of the angular momentum from $l_z = -3$ to 3. Thus 14 electrons can occupy the $4f$ spin-orbitals.

If n electrons are occupied in the $4f$ sub-shell, the number of possible configurations is given by ${}_nC_{14} = \dfrac{14!}{n!(14-n)!}$. These configurations can not be equivalent in the existence of Coulomb interactions between $4f$ electrons, and depend on L and S. Here the norm of the total orbital-angular momentum, L, and of the total spin-angular momentum, S, for the $4f$ electrons are defined as

$$\begin{aligned} L = |\mathbf{L}| \quad &\text{and} \quad S = |\mathbf{S}|, \\ \mathbf{L} = \sum_{\mathrm{i}}^{\mathrm{n}} \mathbf{l}_{\mathrm{i}} \quad &\text{and} \quad \mathbf{S} = \sum_{\mathrm{i}}^{\mathrm{n}} \mathbf{s}_{\mathrm{i}}, \end{aligned} \tag{2.1}$$

where $\mathbf{l}_{\mathrm{i}}$ and s_{i} are the angular and spin-angular momentum for i-th electron, respectively. We write the Hamiltonian for a free ion,

$$H = -\frac{\hbar^2}{2m}\sum_i^n \Delta_i - \sum_i^n \frac{Ze^2}{r_i} + \sum_{i>j}^n \frac{e^2}{|r_i - r_j|} + \lambda \mathbf{L}\cdot\mathbf{S}, \tag{2.2}$$

where λ is a spin-orbit constant. The first and the second terms of (2.2) represent kinetic and potential energies for the i-th electron, respectively. The third and the forth terms represent Coulomb and spin-orbit interactions, respectively. L and S are preserved here if we neglect the spin-orbit interaction. The multiplet terms split by Coulomb interaction can be denoted by ${}^{2S+1}L$, which is called Russell-Saunders coupling. Each of the multiplets denoted by ${}^{2S+1}L$ are degenerate in $(2S+1)(2L+1)$ -fold. In Table 2.1, the appearances of the multiplet terms for the $4f^n$ configurations are listed.

When we consider spin-orbit interactions, the total angular momentum $\mathbf{J} = \mathbf{L} + \mathbf{S}$ only commutes with the above Hamiltonian. Thus, the total angular momentum J preserves in a free atom and the multiplet terms can be represented by ${}^{2S+1}L_J$. The degeneracy of ${}^{2S+1}L_J$ is $2J+1$.

The multi-electron wavefunctions under the spin-orbit coupling are no longer pure Russell-Saunders wavefunctions specified by S and L, but a linear combination of the wavefunctions with the same total angular momentum J. For example, the many-electron wavefunction for the multiplets of Er^{3+} ion (n=11), $\Phi(J=\frac{15}{2})$, is expressed as follows [32],

$$\Phi(J=\frac{15}{2}) = C_1\phi(^4I_{\frac{15}{2}}) + C_2\phi(^2K_{\frac{15}{2}}) + C_3\phi(^2L_{\frac{15}{2}}), \tag{2.3}$$

where $\phi(^{2S+1}L_{\frac{15}{2}})$ is the wavefunction of a pure Russell-Saunders state with $L = L, S = S, J = \frac{15}{2}$. The coefficients C_1, C_2, C_3 are determined by diagonalization of Hamiltonian with the basis functions of $\phi^{\nu}(^{2S+1}L_J)$ which corresponds to each configuration specified by ν. This diagonalization is called configuration interaction (CI) calculation when we calculated the energy matrix elements not only those of one-electron energies but also within two-electron interactions. Especially, the coupling of configurations with the same J by spin-orbit interaction is called intermediate coupling.

The ground state $^{2S+1}L_J$ for an atom is characterized by Hund's rule as follows, (1) the maximum value of the total spin S allowed by the exclusion principle, (2) the maximum value of the orbital angular momentum L consistent with S, (3) the value of J is $|L-S|$ when the shell is less than half filled and to $L+S$ when more than half filled. According to Hund's rule, the multiplet terms for the ground state of rare earth neutral atoms and trivalent ions are listed in Table 2.2 as well as their configurations.

The crystal field splittings are observed when rare earth atoms are in solids. In Fig. 2.1, the multiplet terms observed in $LaCl_3$ are shown [33]. The observed energy levels are measured in the unit of cm^{-1} from

Table 2.1: The multiplet terms for the configurations $4f^n$. The characters $S, P, D, F, G, H, I, K, L, M, N, O, P, Q$ denote L=0, 1, 2, 3, 4, 5, 6, 7, 8, 9, 10, 11, 12, 13, 14 states, respectively.

f^1,f^{13}	^2F			
f^2,f^{12}	^1SDGI	^3PFH		
f^3,f^{11}	$^2PDFGHIKL$	^4SDFGI		
f^4,f^{10}	$^1SDFGHIKLN$	$^3PDFGHIKLM$	^5SDFGI	
f^5,f^9	$^2PDFGHIKLMNO$	$^4SPDFGHIKLM$	^6PFH	
f^6,f^8	$^1SPDFGHIKLMNQ$	$^3PDFGHIKLMNO$	$^5SPDFGHIKL$	^7F
f^7	$^2SPDFGHIKLMNOQ$	$^4SPDFGHIKLMN$	^6PDFGHI	^8S

Table 2.2: The multiplet terms for the ground states of rare earth ions and atoms.

Ion	Configuration	Ground state	Atom	Configuration	Ground state
Ce^{3+}	$4f^15s^2p^6$	$^2F_{\frac{5}{2}}$	Ce	$4f^25s^2p^66s^2$	$^3H_4$
Pr^{3+}	$4f^25s^2p^6$	$^3H_4$	Pr	$4f^35s^2p^66s^2$	$^4I_{\frac{9}{2}}$
Nd^{3+}	$4f^35s^2p^6$	$^4I_{\frac{9}{2}}$	Nd	$4f^45s^2p^66s^2$	$^5I_4$
Pm^{3+}	$4f^45s^2p^6$	$^5I_4$	Pm	$4f^55s^2p^66s^2$	$^6H_{\frac{5}{2}}$
Sm^{3+}	$4f^55s^2p^6$	$^6H_{\frac{5}{2}}$	Sm	$4f^65s^2p^66s^2$	$^7F_0$
Eu^{3+}	$4f^65s^2p^6$	$^7F_0$	Eu	$4f^75s^2p^66s^2$	$^8S_{\frac{7}{2}}$
Gd^{3+}	$4f^75s^2p^6$	$^8S_{\frac{7}{2}}$	Gd	$4f^75s^2p^6d^16s^2$	^9D
Tb^{3+}	$4f^85s^2p^6$	$^7F_6$	Tb	$4f^85s^2p^6d^16s^2$	^8H
Dy^{3+}	$4f^95s^2p^6$	$^6H_{\frac{15}{2}}$	Dy	$4f^{10}5s^2p^66s^2$	$^5I_8$
Ho^{3+}	$4f^{10}5s^2p^6$	$^5I_8$	Ho	$4f^{11}5s^2p^66s^2$	$^4I_{\frac{15}{2}}$
Er^{3+}	$4f^{11}5s^2p^6$	$^4I_{\frac{15}{2}}$	Er	$4f^{12}5s^2p^66s^2$	$^3H_6$
Tm^{3+}	$4f^{12}5s^2p^6$	$^3H_6$	Tm	$4f^{13}5s^2p^66s^2$	$^2F_{\frac{7}{2}}$
Yb^{3+}	$4f^{13}5s^2p^6$	$^2F_{\frac{7}{2}}$	Yb	$4f^{14}5s^2p^66s^2$	$^1S_0$

Figure 2.1: Observed energy levels of the trivalent rare earth ions [33].

the ground states of the multiplets.

2.1.2 EL and PL experiments

The excitation mechanism of $4f$ electrons is discussed by comparing electroluminescence with photoluminescence experiments. The observed electroluminescence (EL) and photoluminescence (PL) spectra of Er doped InP are shown in Fig. 2.2 and Fig. 2.3, respectively [9, 10, 11]. The luminescence at 1.54 μm corresponds to the transition from the first excited state $^4I_{\frac{13}{2}}$ to the ground state $^4I_{\frac{15}{2}}$ of Er^{3+} ions. The 0.9 μm luminescence, which can be observed only in EL experiments, is assigned to the transition from the second excited state $^4I_{\frac{11}{2}}$ to the ground state $^4I_{\frac{15}{2}}$. A schematic view of the luminescence transitions for Er^{3+} is shown in Fig. 2.4.

The EL spectra depend on the applied voltage. In Fig. 2.2, we compare EL spectra at 77 K (a) with that at 300 K (b). The broad peak near 1.2 μm, which is observed at 77 K, disappears at 300 K. It is because non-radiative transitions accompanied with phonons are dominant at high temperature. The broad peak comes from transitions in the host semiconductor. On the other hand, the sharp spectra at 0.9 and 1.54 μm can be observed even at 300 K, though the intensities are reduced by about a half. The luminescence spectra at 0.9 and 1.54 μm do not depend on temperature compared with the broad peak. Thus, the sharp spectra are considered to correspond to the intra-transitions of $4f$ electrons.

As for the PL spectra, the sharp luminescence lines are observed with the broad line of semiconductor, too, at low temperature of 77 K as is shown in Fig 2.3. On the other hand, at room

Figure 2.2: EL spectra at 77 K (a) and 300 K (b) [9].

Figure 2.3: PL spectra at 77 K [9].

Figure 2.4: Schematic multiplet structures of Er^{3+}.

temperature 300 K, both of the sharp and broad peak spectra disappear simultaneously. This shows that the sharp spectra are considered to be occurred by the energy transitions from the host InP to $4f$ electrons due to the recombinations of electron-hole pairs in the semiconductor.

Figure 2.5: The L-V spectra [9].

Further, the relation between the electro-luminescence intensity and the applied voltage (L-V) in the EL experiment is shown in Fig. 2.5.

The 1.54 μm luminescence of ${}^4I_{\frac{13}{2}} \rightarrow {}^4I_{\frac{15}{2}}$ begins rapidly at 7 V and the 0.9 μm luminescence begins at 10 V. The ratio of the two thresholds voltage is nearly equal to the ratio of the peak energies of the two multiplet terms. From the results of Fig. 2.2 and Fig. 2.5, they concluded that the electroluminescence spectra are caused by the direct excitation of $4f$ electrons by free electrons. Thus, the excitation mechanisms of PL and EL are considered to be different, though $4f$ electrons are excited in both experiments.

2.2 Review of *ab initio* calculations for f-electrons

Next, we survey *ab initio* calculations especially for f-electrons which have been developed in the history of quantum chemistry. *Ab initio* calculations are useful to analyze electronic structure because of the excellent reliability of the calculations without any artificial parameters. They have been applied to the calculations of multiplets for many clusters or molecules. However, reports for $4f$ electrons by *ab initio* methods are not so many since *ab initio* calculations for $4f$ electrons exceeds the allowance of facility of computations. In recent years, a rapid progress of computations and theoretical methods has enabled us to perform *ab initio* calculations for a cluster containing a heavy rare earth atom [28].

2.2.1 Quasi-relativistic DV-Xα and MS-Xα methods

At an early stage, theoretical investigations for the electronic structure of f-electrons were performed by the one-component relativistic discrete variational (DV) Xα method [34] and the non-relativistic multiple scattering (MS) Xα method with relativistic corrections [35]. These methods have been applied to the molecule of UF_6.

The formulation of the relativistic DVXα method is based on the Dirac equation with a Xα potential within local density approximation (LDA). The Dirac's Hamiltonian to be solved is,

$$H = c\underline{\alpha}\mathbf{p} + \underline{\beta}mc^2 + V(\mathbf{r}), \tag{2.4}$$

where, c is the velocity of light and $\mathbf{p}$ is the momentum operator. The 4×4 dimensional matrices $\underline{\alpha}_k$ and $\underline{\beta}$ are defined by,

$$\underline{\alpha}_k = \begin{pmatrix} 0 & \underline{\sigma}_k \\ \underline{\sigma}_k & 0 \end{pmatrix}, \quad \underline{\beta} = \begin{pmatrix} \underline{I} & 0 \\ 0 & -\underline{I} \end{pmatrix}, \quad (k = x, y, z) \tag{2.5}$$

where $\underline{\sigma}_k$ is the Pauli's matrices and $\underline{I}$ is the two-dimensional unit matrix. The potential V($\mathbf{r}$) is a sum of the Coulomb direct and exchange-correlation potentials, in which a Xα potential is adopted as the exchange-correlation potential.

For cluster calculations, the wavefunctions have a form of an linear combination atomic orbital (LCAO). The relativistic wavefunctions for the Dirac's Hamiltonian have four components corresponding to the matrix elements in eq. (2.4). The atomic orbitals (AO's) are obtained by solving the atomic Dirac-Slater equation for each atom. Since the fully relativistic DVXα method is not easy to solve the four components of eigenfunctions for clusters, a quasi-relativistic DVXα method is presented [34], in which non-relativistic wavefunctions are used and the quasi-relativistic one-electron energies are obtained by adding the relativistic corrections of mass-velocity, Darwin and SO interaction terms.

In the scattered wave MSXα method, the molecular orbitals (MO's) can be roughly regarded as having an LCAO form but the component AO's are truncated at the respective muffin-tin sphere boundaries. The AO's are joined together by approximate free-electron type solutions between the sphere [35]. The relativistic corrections (mass-velocity and Darwin terms) are added to the non-relativistic Hamiltonian. Level shifts of the one-electron orbitals due to the relativistic corrections are showed. As a result, the one-electron energy gap between the highest occupied molecular orbital (HOMO) and the lowest occupied molecular orbital (LUMO) became wider by the SO effect. The calculated one-electron binding energies agree well with the photo-ionization spectrum which corresponds to the excitations from $2p$ orbitals of fluorine atoms to unoccupied $5f$ orbitals of uranium. There is an overall agreement between the calculated one-electron transitions and the absorption spectrum and this shows that the relativistic effects are important for clusters containing heavy atoms.

The fully relativistic self-consistent Dirac-Slater (DS) model, in which an exchange-correlation interaction is considered in the Xα potential within the local density approximation (LDA), has been used to calculate one-electron energy levels and charge distributions for UF_6 [34]. In the paper, the ionicity of fluorine was calculated by Mulliken's gross population analysis for the ground state of UF_6. From the calculated results of the one-electron energy and charge distribution, they concluded that a free ion basis was not so good as an atomic basis in representing the ground state MO's [34]. Further they performed self-consistent "transition-state" calculations of the intermediate configurations to determine the transition type of the component (f, p, d) for the charge transfer transitions of UF_6. Experimental observed optical and ionization values are interpreted in the theoretical predictions of electronic spectra with a reasonable success.

When we discuss the hybridized chemical bonding structures of $4f$ orbitals with other atoms, the relativistic effect is not always important. The methods based on non-relativistic formula have been successful as follows. A non-relativistic discrete variational Xα (DV-Xα) method is applied to rare earth oxides [14, 15]. Calculated one-electron MO's for chemical trends of rare earth oxides well explain XPS spectra which are in the order of several tenths of eV, corresponding to the excitation from $4f$ to other orbitals of oxygen. The application of non-relativistic DVXα cluster method to rare earth ions (Er^{3+} and Yb^{3+}) in semiconductors (InP, GaP and GaAs) was performed [36] by R. Saito and T. Kimura. They showed the rare earth impurity acceptor levels in the energy gaps of host semiconductors.

2.2.2 Effective core potential method

The *ab initio* calculations for f electrons employing Gaussian basis sets, relativistic effective core potentials and an effective spin-orbit operator have been carried out to characterize the valence charge transfer electronic excitations in UF_6 [37].

In the *ab initio* Hartree-Fock method the exchange non-local integral is explicitly evaluated and the self-energy of an electron is automatically excluded in the exchange term. Thus the exchange potential has a correct form of $N-1$ body operator. On the other hand, Xα approach employs the local density ($\rho^{\frac{1}{3}}(r)$) exchange approximation, where $\rho(r)$ is the charge density at the position r for N electron system, and the self-energy for an electron can not be excluded in the exchange term. Thus, the local density potential has a form of N body operator. In the case of electronic structure of crystals, the difference between $N-1$ and N is not so important since the wavefunction is delocalized. On the other hand, in the case of the localized $4f$ electrons, the self-energy correction may be large.

In the paper [37], the dipole-allowed or dipole-forbidden states are calculated using many-electrons CI wave-functions in the presence of spin-orbit coupling in order to explain the mechanism of charge transfer electronic transition. The observed spectra are assigned to the calculated dipole-allowed or dipole-forbidden excitations between many-electrons orbitals.

A Hartree-Fock (HF) equation for all electrons is theoretically derived from a Hamiltonian for many electrons by variation principle. HF equation has been developed in quantum chemistry and has given successfully reasonable results. However, the SCF calculations for a large number of electrons take too much computational time. In order to solve the time problem, a useful method using a effective core potential (or pseudo potentials) is proposed and is described bellow.

The effective core potential plays an important role for both the economical and reliable calculations. The concept of a effective core potential is to introduce the effects of core electrons in the potential formula. The aim of this method is to reduce computations without considering the core electrons explicitly in SCF calculations. In the study of the electronic structures, valence electrons mainly contribute to the chemical bonding of system. Thus, the valence electrons should be considered as explicitly as possible in first principle method. While, core electrons do not have a large influence on chemical properties. The various types of effective core potentials have been developed by some researchers [38, 39].

In the effective core method, the core electrons of atoms are substituted for the effective core potentials, $u_{\rm eff}$. The Coulomb interactions between core-core and core-valence electrons are effectively included in the potentials. The pseudo-valence Hamiltonian $H_{\rm pv}$, includes explicitly the Coulomb interactions between valence electrons. The interactions between valence and core electrons are included in the effective core potential as well as in the Coulomb interactions between core electrons. The valence Hamiltonian is given as follows,

$$H_{\rm pv} \approx -\sum_{i}^{n_v} \frac{1}{2}\Delta_i + u_{\rm eff}(r_i) + \sum_{i>j}^{n_v} \frac{1}{r_{i,j}}, \tag{2.6}$$

where n_v is the number of valence electrons. The effective core potential $u_{\rm eff}$ reflects the orthogonality of valence electrons to core ones. The effective core potentials are developed in various methods [40, 41] in which the potential is calculated so as to obtain the nodeless pseudo-valence orbitals. The effective core potentials for rare earth atoms were presented by Dolg *et al.* [39]. The effective core potential used in their work has a semi-local pseudopotential in the following form,

$$u_{\rm eff}(r_i) = -\frac{Q}{r_i} + \sum_{l} A_l \exp(-a_l r_i^2) P_l. \tag{2.7}$$

The quantity Q denotes the effective charge of core, i is an electron index. The notation P_l is the projection operator onto the Hilbert subspace with angular symmetry l,

$$P_l = \sum_{m_l} |lm_l >< lm_l|. \tag{2.8}$$

The parameters A_l and a_l (l=0,1,2,3) have been adjusted in numerical HF calculations so as to reproduce the total energies of 10 valence states denoted by LS with use of least squares method. The relativistic effects are included in these parameters by adjusting them to quasi-relativistic HF results.

A convenient form of a spin-orbit operator to be applied in molecular calculations has been proposed [42] as follows.

$$H_{\mathrm{SO}} = \sum_{l=1}^{3} [2\Delta V_l(r)(2l+1)] P_l \; \mathbf{l} \cdot \mathbf{s} \; P_l, \tag{2.9}$$

with

$$\Delta V_l(r) = V_{l,l+\frac{1}{2}}(r) - V_{l,l-\frac{1}{2}}. \tag{2.10}$$

The difference $\Delta V_l(r)$ of the relativistic potentials between $V_{l,l+\frac{1}{2}}$ and $V_{l,l-\frac{1}{2}}$ was parametrized in the form,

$$\Delta V_l(r) = B_l \, \exp(-a_l r^2). \tag{2.11}$$

The exponents a_l have been set equal to the exponents of the pseudopotentials. The coefficients B_l have been adjusted in numerical pseudopotential calculations for the one-valence-electron ions to reproduce the SO splittings derived from corresponding all electron Dirac-Fock (DF) calculations. In Table 2.3, we show these A_l, B_l, a_l parameters for neutral lanthanide atoms [39]. Excitation and ionization energies calculated with the pseudopotentials agree with the corresponding all electron values to better than 0.1 eV for all reference states. In order to test the reliability of the method, the multiplet energies for a Ce^{3+} ion were calculated with the derived SO and quasi-relativistic pseudopotentials. The pseudopotential results are compared with experimental data [43], numerical all-electron values from relativistic DF calculation [44], quasi-relativistic Wood-Boring (WB) [35, 45] and non-relativistic Hartree-Fock (HF) calculations [39, 46] and are shown in Table 2.4. The atomic parameters both in pseudopotentials and in SO splittings are in satisfactory agreement with corresponding all-electron values.

2.2.3 Hartree-Fock and SOCI

A Hartree-Fock equation is derived with the variation principle applied to the Schrödinger equation for many electrons. The one-electron orbitals are determined by self-consistent field Hartree-Fock (SCF-HF) approach. The obtained one-electron orbitals do not include completely the electronic correlation which is known as the correlation effect of electrons. In the configuration interaction (CI) method, the correlation effect is included in the multi-configuration wavefunctions in which electronic excitations from the SCF ground state to unoccupied orbitals are considered. The multi-configuration states are expressed by a liner combination of various configuration state functions and the coefficients of linear combinations are determined by the variation method. Spin-orbit splitting energies for many-electrons are calculated using the multi-configuration state functions as basis sets. Since we use this approach in the present thesis, details of Hartree-Fock and SOCI will be discussed in the next chapter.

Table 2.3: Parameters (in atomic unit) of the quasirelativistic Wood-Boring (WB) pseudopotentials and corresponding spin-orbit (SO) operators.

Table 2.4: Energy levels (cm^{-1}) of the Ce^{3+} ion from experimental results and numerical relativistic (DF), quasirelativistic (WB) and nonrelativistic (HF) all-electron calculations in comparison to pseudopotential (PP) results applying the spin-orbit operator in first order perturbation theory.

2.2.4 Dirac-Fock method

In 1992, a fully relativistic all electron Dirac-Fock calculation was performed by Visser *et al.*[28]. In their work, the Dirac-Fock equations are solved for four component spinors of Gaussian basis functions. In the step of CI method, the complete excitations of valence electrons in the open-shell to a small set of the open-shell spin-orbitals is considered as the Complete Open-Shell CI (COSCI). This method has been applied to an ${EuO_6}^{9-}$ cluster, in which Eu^{3+} ion occupies a strict center of O_h, embedded in the Madelung potential of the rest crystals. The calculated multiplets for (1) a free Eu^{3+} ion, (2) an Eu^{3+} ion embedded in the Madelung potential (MP) and (3) an ${EuO_6}^{9-}$ cluster and (4) an ${EuO_6}^{9-}$ cluster embedded in the MP are shown in Table 2.5. The dominant luminescence transitions occurring in this system are basically the atomic $^5D_0 \rightarrow ^7 F_1$ and $^5D_0 \rightarrow ^7 F_2$ transitions. In these multiplets, the crystal field splitting energies are somewhat overestimated (251 cm^{-1}) by the Madelung potential. Inclusion of the neighboring O^{2-} ions reduce the splitting to 110 cm^{-1}. On the other hand, the calculated splitting between ^5D and ^7F levels is too much large in all calculations compering the experimental values. For the $^5D_0 \rightarrow ^7 F_1$ transition, the theoretical results have a discrepancy with experimental result of $\sim$ 3000 cm^{-1}. They explained that the large error could not be attributed to defects of the basis set or COSCI approach but might be caused by the insufficient correlation effects in the theory.

In summary of this chapter, we review the experimental and theoretical backgrounds relevant to the field of rare earth ions. Especially, we have developed a first principle calculation which considers many interactions without any assumptions. As we can see in this chapter, the many past attempts to calculate the electronic structures of $4f$ electrons have still ambiguities in basis sets and shape of the potentials. In order to remove the ambiguity, many investigation is necessary from different points of view.

The method that we adopt in the present thesis is one of the most sophisticated methods for a large scale computation. In the next chapter, we will describe the details of the present method.

Table 2.5: The Multiplet energies by Fock-Dirac (FD) complete open-shell CI (COSCI) in atomic unit of the lowest states of the f^6-manifold with their degeneracies.

Chapter 3

Method of Calculation

3.1 Introduction

In this chapter, we present the method of the *ab initio* calculation with spin-orbit (SO) interaction. In this thesis, we calculate the multiplet terms of trivalent lanthanide ions and of a cluster containing of a Tm^{3+} ion and neighboring tetrahedral four P atoms. The application of the *ab initio* method based on quantum chemistry to the solid state physics is valid only for the calculation of the localized electronic structures of impurity states. There are some points to be investigated in the computational calculation of the electronic structures of $4f$ electrons systematically, as is discussed in the previous chapter. Especially, we consider the problems of the spatial symmetry of open-shell $4f$ molecular orbitals and relativistic effect on the multiplet terms of rare earth ions, which will be explained in the following.

In section 3-2, we describe the spin-orbit interactions and the method to obtain the effective nuclear charge. The SO interaction is essential for determining the multiplet structures of rare earth ions. In the case of an atom, a quantum mechanical treatment based on the relativistic Dirac equation leads to the SO interaction automatically. Though the present *ab initio* calculation is not available for the relativistic formula in a Hartree-Fock-Roothaan SCF equation, a special treatment is proposed in order to include relativistic effect in SOCI calculation with use of the effective nuclear charge of rare earth ions for $4f$ electrons. A simple method is adopted for obtaining the relativistic effective nuclear charge with use of an atomic Dirac-Slater equation.

In section 3-3, we explain the Gaussian basis sets which are adopted as basis functions of atomic orbitals. We use the Gaussian basis sets obtained by Huzinaga [62] in the thesis. The contraction of the basis set for $4f$ orbitals is the most important concept in the present calculations. The physical meaning of the contraction for $4f$ radial function is also described in this section. In the present calculations, a new mean of contractions for the $4f$ radial function is proposed. Finally, we tabulate the Gaussian basis sets obtained by Huzinaga in the appendix.

In section 3-4, the SCF method for one-electron orbitals is presented. In the case of free ions, the one-electron energies of spherical symmetric $4f$ orbitals are equivalent. Thus, the two electron interactions for the $4f$ electrons are also equivalent with each other. An "open-shell energy coefficient" is used in Coulomb and exchange integrals in Fock operator for the open-shell molecular orbitals in order to satisfy the spatial symmetry especially for the open-shell $4f$ orbitals. We have calculated the open-shell energy coefficient for $4f$ electrons and applied to the present calculations.

In section 3-5, basis sets for configuration interaction are explained. Terminology of CI basis function is also given. Selection of excited levels in CI expansions is important in order to investigate the mechanism of multiplet structures of $4f$ electrons, which is given in this section. Among possible configurations, the interactions between $4f$ electrons are the strongest. Other interactions included in the CI calculation are single and double excitations of valence electrons to unoccupied states.

Finally, in section 3-5, the flow chart of this *ab initio* and the relevant calculations is shown.

3.2 Spin-orbit interaction

Dirac has developed a theory of the electron in the electromagnetic field which satisfies the relativistic requirement of invariance under Lorenz transformation. In the theory, the spin is not introduced *ad hoc* but is given as a consequence of the relativity requirement. The total angular momentum $\mathbf{J} = \mathbf{L} + \mathbf{S}$ commutes with Dirac's Hamiltonian. It is known that the SO interaction, which is specified by J, is important as a relativistic effect for heavy atoms. The relativistic effect becomes negligible when the large kinetic energy cp approaches to the order of the electronic rest energy $mc^2 \sim 500{,}000$ eV. For example, the $1s$ electrons in Tm^{3+} have a kinetic energy of 67,000 eV, which is 13 % to the rest energy. Thus the relativistic treatment can not be avoided for the electrons in rare earth ions.

3.2.1 General expressions of the spin-orbit interaction

A microscopic Breit-Pauli form of SO Hamiltonian for an atom, which can be derived from more rigorous Dirac-Breit Hamiltonian, consists of “spin-own-orbit” and “spin-other-orbit” terms [47, 48, 49]. We use atomic unit unless otherwise noted. The “spin-own-orbit” term is given by,

$$H^{\mathrm{so}}(\mathrm{I}) = \frac{\alpha^2}{2}\sum_i (\mathbf{E}_i \times \mathbf{p}_i)\cdot\mathbf{s}_i = \frac{\alpha^2}{2}\sum_i \left\{ (\frac{Z}{r_i^3}\mathbf{r}_i - \sum_{j\neq i}\frac{\mathbf{r}_{ij}}{r_{ij}^3}) \times \mathbf{p}_i) \right\}\cdot\mathbf{s}_i, \quad (3.1)$$

where

$$\mathbf{E}_i = Z\frac{\mathbf{r}_i}{r_i^3} - \sum_{j\neq i}\frac{\mathbf{r}_{ij}}{r_{ij}^3}, \quad (3.2)$$

is the nuclear electric field for the i-th electron partially shielded by the other electrons. $\mathbf{E}_i$ can be expressed as $\mathbf{E}_i = \nabla_i v(\mathbf{r}_i)$, with the potential $v(\mathbf{r}_i)$ being

$$v(\mathbf{r}_i) = -\frac{Z}{r_i} + \sum_{j\neq i}\frac{1}{r_{ij}}, \quad (3.3)$$

and $r_{ij} = |\mathbf{r}_{ij}| = |\mathbf{r}_i - \mathbf{r}_j|$, and $r_i = |\mathbf{r}_i|$. The quantity α is a fine structure constant, and $\mathbf{p}_i$, $\mathbf{s}_i$ and $\mathbf{l}_i$ are the linear momentum, spin and orbital angular momenta for the i-th electron, respectively. Z denotes the nuclear charge of the atom. It should be noted that, if the central-field model is applied to the electric field in eq.(3.1), then the potential $v(\mathbf{r}_i)$ depends only on the radial coordinate r_i and the following simplification can be achieved with the central field potential $u(r_i)$.

$$H^{\mathrm{so}}(\mathrm{I}) = \frac{\alpha^2}{2}\sum_i (\nabla_i v(\mathbf{r}_i) \times \mathbf{p}_i)\cdot\mathbf{s}_i = \frac{\alpha^2}{2}\sum_i (\frac{1}{r_i}\frac{du(r_i)}{dr_i})\mathbf{l}_i\cdot\mathbf{s}_i. \quad (3.4)$$

The “spin-other-orbit” term is given by,

$$H^{\mathrm{so}}(\mathrm{II}) = -\alpha^2\sum_{i\neq j}\frac{1}{r_{ij}^3}(\mathbf{r}_{ij} \times \mathbf{p}_i)\cdot\mathbf{s}_j, \quad (3.5)$$

which represents a magnetic interaction between the spin motion of an electron and the orbital motion of the other electrons, and originates from the Breit correction term [47]. Of the two terms, the relative importance of the latter in the total SO splitting is known to decrease as the atom becomes heavier [50, 51] and we neglect this term completely in the present study. Recognizing that the two-electron part of $H^{so}(\mathrm{I})$ represents the screening of the nuclear charge Z, an approximate one-body SO Hamiltonian was suggested,

$$H^{\mathrm{so}}(\mathrm{approx}) = \frac{\alpha^2}{2} \sum_i \frac{Z_{\mathrm{eff}}}{r_i^3} \mathbf{l}_i \cdot \mathbf{s}_i, \tag{3.6}$$

which can be obtained using the simple Coulombic potential $u(r_i) = -\frac{Z_{\mathrm{eff}}}{r_i}$ in eq. (3.4). Here, Z_{eff} is called effective nuclear charge for spin-orbit interaction. This approximate form has been widely used because of the simplicity of the calculations [48, 52].

As is well known [53, 54], relativistic effects, mostly mass-velocity effect, cause the contractions of inner s and p orbitals. Because of the more effective nuclear shielding by the contracted inner s and p orbitals with relativistic effects, we expect Z_{eff} would becomes smaller relative to that obtained non-relativistically and the $4f$ orbitals would expand outwards. Thus we expect a smaller value of the SO splitting of the multiplet. In the present method, we calculate the changes of orbital sizes by adopting atomic Dirac-Slater (DS) method [55, 34] and investigate the relativistic effects on the SO multiplet energies for trivalent rare earth ions.

3.2.2 Effective nuclear charge

As far as we found in the literature, most of the calculations with the approximate one-body spin-orbit Hamiltonian H^{so}(approx) have treated Z_{eff} as an adjustable parameter so determined as to reproduce the experimental SO splitting energies [37, 56, 57, 58]. However, we have shown that the multiplet terms constructed by SO interactions for rare earth ions are sensitive to the Z_{eff} value [59]. Moreover, especially for rare earth ions, lots of multiplet terms are experimentally observed due to the complexity of the $4f$ splitting pattern. It is therefore worthwhile to obtain Z_{eff} without any assumptions. For heavy rare earth atoms, it is important to compare Z_{eff} determined by relativistic and non-relativistic method, as described above. For this purpose, we adopt both atomic Dirac-Slater equation and non-relativistic Xα Schrödinger equation in the present thesis.

The Dirac's equation to be solved is ;

$$\begin{aligned} H\varphi_{n\kappa\mu}(\mathbf{r}) &= (c\underline{\alpha}\mathbf{p} + \underline{\beta}mc^2 + u_0(r))\varphi_{n\kappa\mu}(\mathbf{r}) \\ &= E_{n\kappa}\varphi_{n\kappa\mu}(\mathbf{r}). \end{aligned} \tag{3.7}$$

The notations in the Hamiltonian are the same as those explained in section 2.2. The Xα atomic core potential $u_0(r)$ is adopted in the present Dirac-Slater and Xα Schrödinger equations and is mentioned in the following. In eq. (3.7), $\varphi_{n\kappa\mu}(\mathbf{r})$ is the relativistic atomic orbital and contains large- $({f_{n\kappa}}^{\mu}(r))$ and small- $({g_{n\kappa}}^{\mu}(r))$ relativistic components with the spin-angular components ${\chi_{\kappa}}^{\mu}(\hat{r})$ and $\chi_{-\kappa}^{\mu}(\hat{r})$, respectively, as following.

$$\varphi_{n\kappa\mu}(\mathbf{r}) = \begin{bmatrix} {f_{n\kappa}}^{\mu}(r){\chi_{\kappa}}^{\mu}(\hat{r}) \\ i{g_{n\kappa}}^{\mu}(r){\chi_{-\kappa}}^{\mu}(\hat{r}) \end{bmatrix}. \tag{3.8}$$

The subscripts n, μ denote the principal quantum number and magnetic quantum number, respectively. The relativistic quantum number κ is defined by

$$\kappa = \begin{cases} -(l+1) = -(j+\frac{1}{2}), & (j = l+\frac{1}{2}) \\ l = j+\frac{1}{2}, \quad (j = l-\frac{1}{2}) \end{cases} \tag{3.9}$$

for up- and down- spins, respectively.

In order to obtain a suitable numerical value for Z_{eff}, we compare eqs. (3.4) and (3.6) and obtain the following formula,

$$Z_{\text{eff}} = \frac{\int_0^\infty \xi(r) R_{4f}(r)^2 r^2 dr}{\int_0^\infty \frac{\alpha^2}{2}\frac{1}{r} R_{4f}(r)^2 dr}, \quad \xi(r) = \frac{\alpha^2}{2}\frac{1}{r}\frac{du_0(r)}{dr}. \tag{3.10}$$

where the radial wavefunction of the $4f$ orbital $R_{4f}(r)$ ($R_{4f}(r)$ corresponds to ${f_{n\kappa}}^{\mu}(r)$) and spherical symmetrized screened atomic potential $u_0(r)$ are obtained by solving both Dirac-Slater (DS) atomic equation and spin-dependent numerical Xα Schrödinger (XS) equation for comparison. In the DS and XS atomic equations, the radial wavefunction $R_{4f}(r)$ and the atomic potential $u_0(r)$ are numerically solved self-consistently within a local density approximation [60]. In the DS method, an atomic potential $u_0(r)$ is adopted in the Dirac's Hamiltonian of eq. (2.4) as follows,

$$u_0(r) = -\frac{Z}{r} + \int \frac{\rho(\boldsymbol{r}_j)}{|r - r_j|} d\boldsymbol{r}_j - 3\alpha_0 (\frac{3}{4\pi}\rho(r))^{\frac{1}{3}}, \tag{3.11}$$

where the quantity Z denotes the bare nuclear charge of rare earth. The last term of eq. (3.11) is a Xα potential [61] which is widely used as an exchange-correlation potential in the local density functional theory [60]. We used the Xα parameter α_0=0.7. Though the selection of α_0=0.7 is not justified for f electrons, it is in the right range [36]. The relative energy between the valence and $4f$ orbitals does not change for α_0 between 0.6 and 0.8. Using atomic solutions and eq. (3.10), we obtain $Z_{\rm eff}$ for each trivalent rare earth ion. In addition to the DS calculation, we have also performed a nonrelativistic Xα calculation and these formulas are identical to the $c = \infty$ limit of the DS code. The obtained $Z_{\rm eff}$ values are used in one-electron spin-orbit Hamiltonian. In the two methods, the $4f$ electrons are set to be put by the Hund's rule.

3.3 Gaussian basis sets

Gaussian-type orbitals (GTO's) are taken as atomic basis sets in COLMBS. We adopt the Gaussian basis sets obtained by Huzinaga [62] in the present calculation. The GTO's for normalized atomic orbitals in the spherical polar coordinate are defined as

$$X_{nlm}(r,\theta,\phi) = R_{nl}(r)Y_{lm}(\theta,\phi), \tag{3.12}$$

where

$$R_{nl}(r) = N(n,\alpha)r^{n-1}\exp(-\alpha r^2),$$

with

$$N(n,\alpha) = 2^{n+1}[(2n-1)!!]^{-\frac{1}{2}}(2\pi)^{-\frac{1}{4}}\alpha^{\frac{(2n+1)}{2}}, n = l+1, l+2, l+3, ... \tag{3.13}$$

and $Y_{lm}(\theta,\phi)$ are spherical harmonic functions. In COLMBS, the Cartesian coordinate expression for a normalized GTO is used;

$$X_{abc}(x,y,z) = N(a,b,c;\alpha)x^a y^b z^c \exp(-\alpha r^2),$$

with

$$N(a,b,c;\alpha) = (\tfrac{2}{\pi})^{\frac{3}{4}}[(2a-1)!!(2b-1)!!(2c-1)!!]^{-\frac{1}{2}}\alpha^{[a+b+c+\frac{3}{2}]/2}. \tag{3.14}$$

It is noted that the power of r in eq. (3.13) is restricted to the lowest for each symmetry, $n = l + 1$, in eq. (3.14). The GTO's both of $X_{abc}(x, y, z)$ and $X_{nlm}(r, \theta, \phi)$ are equivalent in the sense that each of the two GTO's are converted to the other one by unitary transformations. The normalization constant $N(a, b, c; \alpha)$ for the Gaussian basis sets $X_{abc}(x, y, z)$ in eq. (3.14) is defined by the integration over both the radial and angular parts. It is noted that the normalization constants for Gaussian basis sets are often defined only for the radial part. For example, the integration about the angular part of s-type functions give the value 4π. Thus, the normalization constant C_s for the s-type primitive Gaussian is defined by

$$C_s{}^2 \int_0^\infty r^2 e^{-2\alpha r^2} dr = \frac{1}{4\pi}, \tag{3.15}$$

thus, the constant C_s is given by

$$C_s = (\frac{2\alpha}{\pi})^{\frac{3}{4}}. \tag{3.16}$$

Thus, the C_s is uniquely determined by the exponent. Hereafter we denote the radial part of $X_{abc}(x, y, z)$ with the exponent α_i as the primitive Gaussian, $g_{\alpha_i}(r)$. The j-th subshell (or j-th atomic orbital), $\varphi_j(r)$, are expressed by the sum of the primitive sets $g_{\alpha_i}(r)$,

$$\varphi_j(r) = \sum_i^{d_0} C_{ji}{}^0 g_{\alpha_i}(r), \tag{3.17}$$

where d_0 is the number of primitive sets and α_i is the exponent of the i-th primitive sets. In this representation, the j-th subshell consists of d_0 basis functions. Since molecular orbitals consist of linear combinations of atomic orbitals, as described bellow, it is required that the number of atomic basis functions is reduced without the precision being kept as well as possible. For that purpose, it is fixed that an atomic basis function consists of plural primitive Gaussians.

$$\varphi_j(r) = \sum_{i=1}^{d_1} C_{ji}{}^{(1)} g_{\alpha_i}(r) + \sum_{i=d_1+1}^{d_2} C_{ji}{}^{(2)} g_{\alpha_i}(r) + .. + \sum_{i=d_{0-1}+1}^{d_0} C_{ji}{}^{(c)} g_{\alpha_i}(r),$$
$$(d_1 < d_2 < .. < d_0) \tag{3.18}$$

where c ($< d_0$) is the number of contracted Gaussian basis sets and the basis functions of the subshell are reduced by $d_0 - c$. The coefficients $C_{ji}{}^{(1)}, C_{ji}{}^{(2)}, ..., C_{ji}{}^{(c)}$ are renormalized in each of the contracted basis functions with the ratios of the coefficients of the primitive sets $C_{j1}{}^0/C_{j2}{}^0, C_{j2}{}^0/C_{j3}{}^0, ..., C_{jd_0-1}{}^0/C_{jd_0}{}^0$ being unchangeable. In the present calculations, we use the contracted GTO's and a molecular orbital Ψ_k is expressed by a linear combination of contracted Gaussian type orbitals φ_j,

$$\Psi_k = \sum_j C_{jk}\varphi_j \tag{3.19}$$

in which the coefficients C_{jk} are determined by solving SCF Hatree-Fock equations. When atomic orbitals φ_j are represented by only one contracted basis set or by two ones, the basis sets are called single-zeta or double-zeta, respectively.

We adopt the Gaussian basis sets proposed by Huzinaga [62] for trivalent rare earth ions and ligand P atoms. In Appendix, the exponents and coefficients for rare earth and phosphorus atoms are listed. It should be mentioned that these basis sets are optimized for for the neutral atoms but for ions. Each of the one-electron orbitals are the contracted single-zeta. More suitable basis sets for ions could be obtained through dividing the contracted one-electron orbitals into double-zeta

Table 3.1: The selection of the contractions.

atomic orbital	$4f$	$4d$	$6s$	RE
number of primitive sets	4	3	3	
Base I	31 (DZ)	3 (SZ)	3 (SZ)	free ions
Base II	4 (SZ)	21 (DZ)	3 (SZ)	free ions
Base III	31 (DZ)	3 (SZ)	not included	$(TmP_4)^{3+}$

* DZ = double zeta, SZ = single zeta

or more primitives and increasing the flexibility of the basis sets. However, there are some ambiguities in selecting the contraction patterns. We tried several selections of the contractions. For realizing ionic states, first, the $4f$ GTO is split to double-zeta and remain the other orbitals as atomic single-zeta, which we hereafter call Base I. Second, the $4d$ GTO is split to double-zeta and the others are single-zeta (Base II). The $6s$ orbital is included in SCF and CI calculations for free ions but removed from the basis sets in the case of $(TmP_4)^{3+}$ cluster (Base III) because no convergence is obtained by the existence of unoccupied $6s$ related MO. For ligand P atoms, three-s type, two-p type and one-d type contracted single-zeta GTO's are used. The selection of the contractions is listed in Table 3.1.

3.4 SCF calculation for one-electron molecular orbitals

Two different physical models of, a cluster containing impurity Tm^{3+} ion and single ions, are calculated by all-electron SCF and SOCI methods.

A cluster of $(TmP_4)^{3+}$ is adopted as a physical model of Tm^{3+} in InP. The atomic distance between Tm^{3+} and P is taken 2.54Å which is the same as that of the InP lattice. As for rare earth ions, six ions with even number electrons, Pr^{3+}, Pm^{3+}, Eu^{3+}, Tb^{3+}, Ho^{3+} and Tm^{3+}, the SOCI calculations are performed. The SOCI calculations for free ions are necessary to show a chemical trend of results obtained by the present *ab initio* method. The relationship between relativistic effect and Gaussian basis sets is also considered from the calculated results of free ions.

3.4.1 Hamiltonian

The Hamiltonian to be solved is ;

$$\begin{aligned} H &= H_0 + H_1 \\ &= \sum_i \left\{ -\frac{\hbar^2}{2m}\nabla_i{}^2 - \sum_a \frac{Z_a e^2}{|R_a - r_i|} + \frac{\alpha^2}{2}\frac{Z_{\mathrm{eff,\ RE}}}{|R_{\mathrm{RE}} - r_i|^3}\mathbf{l}_i \cdot \mathbf{s}_i \right\} \\ &+ \sum_{<i,j>} \frac{e^2}{|r_i - r_j|} \end{aligned} \tag{3.20}$$

where α is the fine structure constant. Z_a and R_a denote the nuclear charge and the position of the a-th atom, respectively. The one-body SO interaction is introduced in the third term of the one-electron Hamiltonian, H_0. The last term, H_1, represents electron-electron interactions. The effective nuclear charge $Z_{\mathrm{eff,\ RE}}$ is determined by solving atomic Dirac-Slater and Xα Schrödinger equations, as was discussed in the previous section. In the present study, the subscript RE of $Z_{\mathrm{eff,\ RE}}$ denotes only the trivalent rare earth ion. In the SCF-HF calculation, the third term of eq. (3.20) is not included, which is considered in SOCI calculation.

3.4.2 Hartree-Fock procedure

In this section, we briefly describe the formulation of Hartree-Fock-Roothaan equation. The MO's are obtained by solving the restricted Roothaan Hartree-Fock equations in which the spin-functions of up- and down- spins are not distinguished in many electrons wave functions. A MO Ψ_i consists of a linear combination of atomic orbitals φ of various quantum numbers on the various atoms.

$$\Psi_i = \sum_{k=1}^{M} C_{ki}\varphi_k. \tag{3.21}$$

The number of atomic basis functions is at least equal to that of total atomic orbitals M and this basis sets are called minimum sets. The same thing is said in an another way, in minimum sets all the atomic orbitals are represented by single-zeta GTO's. In order to increase the flexibilities of the MO's, the contracted GTO's should be splitted into double-zeta's or more than those. Then, the basis sets become larger than the atomic orbitals. In fact, these operations for the contracted GTO's, especially for $4f$ GTO's, occurs a serious problem. That is to say, there is a relationship between the contractions and the relativistic effect on $4f$ radial functions as is described in the latter chapter. The atomic orbitals φ_k on the different atoms are not orthogonal each other. The overlap integral between two AO's is written by

$$S_{nk} = \int \varphi_n{}^*(1)\varphi_k(1)d\mathbf{r_1}. \tag{3.22}$$

The total wavefunction for many electrons is represented by the determinantal function in terms of the MO's. A Hatree-Fock-Roothaan equation for i-th MO is,

$$f(1)\sum_{k=1}^{M} C_{ki}\varphi_k(1) = \epsilon_i \sum_{k=1}^{M} C_{ki}\varphi_k(1), \tag{3.23}$$

where the Fock operator for a electron 1, $f(1)$, is written by

$$f(1) = h(1) + \sum_{k'=1}^{M} \int d\mathbf{r_2}\varphi_{k'}{}^*(2) r_{12}^{-1}(1 - P_{12})\varphi_{k'}(2), \tag{3.24}$$

and here $h(1)$ is a one-electron Hamiltonian and P_{12} is a operator which permutes the positions of the two electrons each other $(1 \leftrightarrow 2)$. The matrix elements of the secular equations for Hartree-Fock-Roothaan equations can be derived from the differential equation of eq. (3.23) by multiplying n-th atomic orbital φ_n and by integrate over the coordinate, then,

$$\sum_{k=1}^{M} C_{ki} \int d\mathbf{r_1}\varphi_n{}^*(1) f(1)\varphi_k(1) = \epsilon_i \sum_{k=1}^{M} C_{ki} \int d\mathbf{r_1}\varphi_n{}^*(1)\varphi_k(1). \tag{3.25}$$

The matrix component of Fock operator is written by

$$F_{\mu\nu} = \int d\mathbf{r_1}\varphi_\mu{}^*(1) f(1)\varphi_\nu(1), \tag{3.26}$$

and the matrix F is Hermitian.

The consecutive Hartree-Fock-Roothaan equations for M MO's can be written by the matrix formula, as follows,

$$\sum_{k=1}^{M} F_{nk}C_{ki} = \epsilon_i \sum_{k=1}^{M} S_{nk}C_{ki} \quad (i = 1, \cdots, M), \tag{3.27}$$

where S, ϵ_i and C_i are the overlap matrix, eigenvalue and coefficient vector of the i-th MO, respectively. The degree M is the number of

MO's and F is Fock matrix which is the sum of the one-electron (F_1) and two-electron (F_2) operators,

$$F = F_1 + F_2. \tag{3.28}$$

The matrix elements of the Fock operators are given by

$$F_{nk} = 2[n|k] + 2\sum_{j=1}^{N}\sum_{p,q=1}^{M} C_{pj}^{*}C_{qj}^{*}\{[nk|pq] - [nq|pk]\}, \tag{3.29}$$

in which,

$$[n|k] = \int d\mathbf{r_1}\varphi_n^{*}(1)[-\frac{1}{2}\nabla_1{}^2 - \sum_a \frac{Z_a}{r_{1a}}]\varphi_k(1) \tag{3.30}$$

$$[nk|pq] = \int d\mathbf{r_1}d\mathbf{r_2}\varphi_n^{*}(1)\varphi_k(1)\frac{1}{r_{12}}\varphi_p^{*}(2)\varphi_q(2). \tag{3.31}$$

The number of MO's is 66 for a $(\mathrm{TmP}_4)^{3+}$ cluster. Since the $4f$ atomic orbital (AO) is partially occupied, special treatment is needed to reproduce the symmetrized $4f$ related MO's in the crystal field. Group III atoms are surrounded by V atoms in the tetrahedral point group, T_d. A trivalent lanthanide is assumed to be at a substitutional site of a group III atom in III-V semiconductors. Although we say InP as a host material, the effect of In atoms at next nearest-neighbor sites is not considered in the *ab initio* calculation because of the capacity. In fact, the previous DV-Xα cluster calculation in which nearest neighbor sites are considered shows that the mixing of the valence orbitals of In atoms on $4f$ orbitals is small [36]. By the same reason, the Madelung potential of the second nearest points may be neglected in the present thesis. Furthermore, the three valence electrons of trivalent ions are removed from the cluster. It was shown by the DVXα calculation [36] that the three valence electrons existed in shallow donor levels and the wavefunction of the donor level was delocalized in larger volume in semiconductors than the size of a cluster which we adopt in the present calculation. In fact, they showed that if the three electrons were put in the cluster, the kinetic energies of the electrons would become much higher than the donor levels. Thus, since the trivalent outer donor electrons do not affect inner $4f$ electrons, we can neglect the existence of the three electrons in the cluster.

Table 3.2: Decomposition irreducible representations of T_d to C_{2v}.

T_d		C_{2v}
A_1	$\Longrightarrow$	A_1
A_2	$\Longrightarrow$	A_2
E	$\Longrightarrow$	$A_1 + A_2$
T_1	$\Longrightarrow$	$A_2 + B_1 + B_2$
T_2	$\Longrightarrow$	$A_1 + B_1 + B_2$

We use the symmetry adapted MO's in the SOCI calculations for the open-shell $4f$ orbitals in order to have the symmetry satisfied multiplet energy levels. Otherwise the use of symmetry-broken orbitals leads to energy splitting lower symmetry than the original T_d symmetry, and makes it impossible to analyze the additional energy splittings caused by the crystal field. In crystal field with a T_d symmetry, the $4f$ orbitals are decomposed into the subspace $A_1 + T_1 + T_2$, where A_1, T_1, T_2 are irreducible representations of T_d. Furthermore, each of the irreducible representations of T_d is decomposed into those of C_{2v} symmetry which we use in the present calculation as shown in Table 3.2, since the computational library COLMBS does not support the point group T_d in

SCF calculations.

3.4.3 Open-shell energy coefficients

Since the valence orbitals are closed-shells in rare earth ions, only the $4f$ orbitals require a special care of open-shell structures. In the case of single rare earth ion, $4f$ AO's should be all degenerate in the spherical symmetric potential. In this case, the Coulomb interactions between $4f$ electrons are equivalent. The "open-shell energy coefficient" is defined for obtaining equivalent electron-electron interactions in the open-shell orbitals.

Open-shell SCF energies in which open-shell Coulomb and exchange energies are given, can be written as follows [63, 64],

$$E_{\mathrm{open-shell}} = \sum_{i}^{\mathrm{open}} N_i H_i + \frac{1}{2} \sum_{i,j}^{\mathrm{open}} N_i N_j (a_{i,j} J_{i,j} - \frac{1}{2} b_{i,j} K_{i,j}), \qquad (3.32)$$

where

$$\alpha_{i,j} = 1 - a_{i,j}, \qquad \beta_{i,j} = 1 - b_{i,j}. \qquad (3.33)$$

Here H_i, $J_{i,j}$ and $K_{i,j}$ are the one-electron, Coulomb and exchange energies, respectively. The summation of Eq.(3.32) is taken only for the open-shell MO's. The coefficients $\alpha_{i,j}$ and $\beta_{i,j}$ are the open-shell energy coefficients [65, 66] which represent the modification of two electron interactions between the open-shells. N_i is the average occupation number of th i-th orbital given by

$$N_i = \frac{n}{n_2}, \qquad (3.34)$$

where n and n_2 are the number of electrons and the number of orbitals in the open-shell, respectively. In the case of $4f$ electrons of rare earth ions, n_2=7 and $n = 1 \sim 13$.

There are two ways to calculate kinds of open shell energy coefficients. One is a set of coefficients for the average-state and the other is for a specified multiplet. The latter is generally determined for the multiplet state named as ${}^{2S+1}L$. On the other hand, the averaged state over all possible multiplets is convenient and adopted in many cases [28].

Here, we use mainly the average-state SCF method. The average-state open-shell energy coefficients is defined as a weighted average of the coefficients on possible multiplets. Furthermore, in order to satisfy the spherical symmetry, each of the open-shell $4f$ orbitals should be equally occupied by $\frac{n}{7}$ electrons, where n is the number of open-shell $4f$ electrons. For a single Tm^{3+} ion, we also calculate the multiplet energies with use of the specified open-shell energy coefficients of ${}^3H$ state, for comparison.

3.5.1 Average state open-shell energy coefficients

In the average-state approximation, the two-electron interaction energy is $\sum_{i,j}(2J_{i,j} - K_{i,j})$ divided by the number of different pairs of $2n_2$ spin-orbitals, i.e. $2n_2(2n_2-1)/2$, while there are $n(n-1)/2$ pairs of electrons. The average total interaction energy E_{av} is therefore given by

$$E = \frac{n(n-1)}{n_2(2n_2-1)} \sum_{i,j}^{open} (J_{i,j} - \frac{K_{i,j}}{2}). \tag{3.35}$$

Comparing Eq. (3.35) with Eq. (3.32) and Eq. (3.34), we have

$$a_{i,j} = b_{i,j} = \frac{2n_2(n-1)}{n(2n_2-1)}. \tag{3.36}$$

Putting $n_2 = 7$ and $n = 12$ in Eq. (3.33) and Eq. (3.36), we get $\alpha = \beta = \frac{1}{78}$. These are the open-shell energy coefficients for the average-

Table 3.3: The open-shell energy coefficients for average-state of trivalent lanthanide ions. In the case of average states, the two coefficients α and β are equal.

ions	Ce^{3+}	Pr^{3+}	Nd^{3+}	Pm^{3+}	Sm^{3+}	Eu^{3+}	Gd^{3+}
n	1	2	3	4	5	6	7
$\alpha = \beta$	1	$\frac{6}{13}$	$\frac{11}{39}$	$\frac{5}{26}$	$\frac{9}{65}$	$\frac{4}{39}$	$\frac{1}{13}$

Ions	Tb^{3+}	Dy^{3+}	Ho^{3+}	Er^{3+}	Tm^{3+}	Yb^{3+}
n	8	9	10	11	12	13
$\alpha = \beta$	$\frac{3}{52}$	$\frac{5}{117}$	$\frac{2}{65}$	$\frac{3}{143}$	$\frac{1}{78}$	$\frac{1}{169}$

state defined by 12 electrons in $4f$ orbitals. We use these values for the average-state of both a single Tm^{3+} ion and a $(TmP_4)^{3+}$ cluster. In Table 3.3 the open-shell energy coefficients of trivalent lanthanide ions for the average states are listed.

3.5.2 ^3H state open-shell energy coefficients

As for the open-shell energy coefficients for the ground state, ^3H state of a Tm^{3+} ion for example, we have the following open-shell energy expression for the two-electron part of the ^3H state for the configuration f^2 [67] p.207,

$$E_{\,^3\mathrm{H},\ \mathrm{f}^2} = F^0 - \frac{1}{9}F^2 - \frac{17}{363}F^4 - \frac{25}{14157}F^6. \tag{3.37}$$

With Eq. (14) of the reference [68], we can convert the expression of f^2 to that of f^{12} as follows,

$$E_{\,^3\mathrm{H},\ \mathrm{f}^{12}} = 66F^0 - \frac{13}{9}F^2 - \frac{347}{363}F^4 - \frac{16525}{14157}F^6. \tag{3.38}$$

Here F^k is Slater's direct integral, which is given by

$$F^k = \int_0^\infty \int_0^\infty \frac{{r_<}^k}{r_>^{k+1}} {R_{4f}}^2(r_1)^2 {R_{4f}}^2(r_2) dr_1 dr_2 \tag{3.39}$$

Then we use the relationship between J, K and F^k. From the discussion in p.177-187 of the reference [67], we know that

$$\sum_{i,j} J_{i,j} = n_2^2 F^0, \sum_{i,j} K_{i,j} = n_2 F^0 + n_2^2 \sum_{k>0} \begin{pmatrix} 3 & 3 & k \\ 0 & 0 & 0 \end{pmatrix}^2 F^k. \tag{3.40}$$

Here the summation for $J_{i,j}$ and $K_{i,j}$ is taken over spatial orbitals and $\begin{pmatrix} 3 & 3 & k \\ 0 & 0 & 0 \end{pmatrix}$ is the Wigner's $3j$ symbol. Putting n_2=7 in eq. (3.40), we get

$$\sum_{i,j} J_{i,j} = 49F^0, \sum_{i,j} K_{i,j} = 7F^0 + \frac{28}{15}F^2 + \frac{14}{11}F^4 + \frac{700}{429}F^6. \tag{3.41}$$

Then Eq. (3.32) is expanded by F^k,

$$E_{\text{open-shell}} = (72a - \frac{36}{7}b)F^0 - \frac{36}{49}b(\frac{28}{15}F^2 + \frac{14}{11}F^4 + \frac{700}{429}F^6). \tag{3.42}$$

Here the subscripts of a and b appeared in eq. (3.32) are not necessary because of the equivalent treatment of the $4f$ orbitals. Finally, comparing Eq. (3.42) with Eq. (3.38), we get the following simultaneous equations;

$$\begin{cases} 72a - \frac{36}{7}b = 66 \\ \frac{36 * 28}{49 * 15}b = \frac{13}{9} \\ \frac{36 * 14}{49 * 11}b = \frac{347}{363} \\ \frac{36 * 700}{49 * 429}b = \frac{16525}{14157} \end{cases} \tag{3.43}$$

It is generally impossible for two variables to satisfy four independent equations. Since F^4 and F^6 are generally smaller than F^0 and F^2, we obtain approximately $a = \frac{857}{864}$ and $b = \frac{455}{432}$ from the first two equations of Eq. (3.43). The corresponding values of α and β are $\alpha = \frac{7}{864}$ and $\beta = -\frac{23}{432}$. These are the open-shell energy coefficients for the approximate ^3H state used for a single Tm^{3+} ion. We observe, however, that these approximate ^3H parameters can not lead to the SCF convergence of a $(TmP_4)^{3+}$ cluster as described above and will give numerical results only for a Tm^{3+} ion for the approximated ^3H state. We confirm that the obtained multiplet energies in a Tm^{3+} ion cause no difference with the both open-shell energy coefficient for the ^3H ground state and for the average state as will be discussed in section 4.3.

3.5 Configuration interaction method

Configuration Interaction (CI) method is a calculation including (1) all the configurations generated in the manifold for the $4f$ electrons ($4f$ full CI or so called Complete Active Space CI (CASCI)) as reference functions and (2) single and double excitations to unoccupied MO's. The CASCI for a partially occupied $4f$ manifold generates a large amount of the reference space and can adopt the spherical symmetry. The many-electron wavefunction, Ψ_{CI}, is given by a linear combination of configuration state functions (CSF's) as follows,

$$\Psi_{\text{CI}} = \sum_{i}^{N} C_i \Phi_i. \tag{3.44}$$

Here N is the number of the CSF's. The i-th CSF's, Φ_i, is a Slater's determinant for the i-th configuration. The CSF's include singly and doubly excited configurations as well as the reference ones, all of which are bound to have singlet or triplet characters in the present study. The coefficient C_i is determined by the linear variational method in the diagonalizations of Hamiltonian.

In order to construct CSF's, we classify all the MO's into five kinds, i.e. (1)doubly occupied, (2)active, (3)external, (4)frozen core and (5)frozen virtual orbitals. A doubly occupied orbital contains two electrons in any reference CSF, and up to two-electron excitations are allowed from the set of whole doubly occupied orbitals. The active orbital can have zero, one or two electrons. The external orbital is unoccupied in any reference CSF, but up to two-electron excitations to the set of whole external orbitals are allowed. The frozen core orbital is always doubly occupied and the frozen virtual orbital is always empty in a CSF.

In the case of Tm^{3+}, the number of reference functions is ${}_{14}C_{12}$=91. All the CSF's generated from these reference functions consist of about 200,000 CSF's in the case of a $(TmP_4)^{3+}$ cluster. A matrix of 200,000 $\times$ 200,000 are effectively diagonalized by decomposing the matrix into the irreducible representations of the point group.

For the present purpose, $4f$-like orbitals are selected as active ones, and the unoccupied virtual f or d orbitals (f^* or d^*) are taken as external ones. We also take the unoccupied $3p$ orbitals of P atoms as external orbitals in the present calculation. All the occupied MO's having lower energies than those of $4f$ orbitals are chosen as frozen core to reduce the number of CSF's. The CI specification of the MO's for the three GTO's given in Table 3.1 is listed in Table 3.5.

Table 3.4: CI basis for RE ions and $(TmP_4)^{3+}$ cluster.

	RE^{3+} with Base I
frozen core	$1s, 2s, 3s, 4s, 5s, 2p, 3p, 4p, 5p, 3d, 4d$
active	$4f$
external	$4f^*$, $6s$
frozen virtual	none

	RE^{3+} with Base II
frozen core	$1s, 2s, 3s, 4s, 5s, 2p, 3p, 4p, 5p, 3d, 4d$
active	$4f$
external	$4d^*$, $6s$
frozen virtual	none

	$(TmP_4)^{3+}$ cluster with Base III.	
	Tm^{3+}	P
frozen core	$1s, 2s, 3s, 4s, 5s, 2p, 3p, 4p, 5p, 3d, 4d$	$1s, 2s, 3s, 2p, 3p$
active	$4f$	none
external	$4f^*$	$3p$
frozen virtual	none	none

3.6 Flow chart of the present calculations

We show the flow chart of the present calculations.

1. Specify rare earth ions. (Ce^{3+}, Pr^{3+}, Nd^{3+}, Pm^{3+}, Sm^{3+}, Eu^{3+}, Gd^{3+}, Tb^{3+}, Dy^{3+}, Ho^{3+}, Er^{3+}, Tm^{3+}, Yb^{3+})

2. Solve the Dirac-Slater equation for a specified ion using the Hamiltonian of eq. (2.4) with the Xα potential of eq. (3.11) and obtain $R_{4f}(r)$ and $u_0(r)$.

3. Calculate Z_{eff} using eq. (3.10).

4. Get the open-shell energy coefficient for the average-state or ${}^3H$ state.

5. Select Basis sets (see section 3.4).

6. Calculate SCF-HF and obtain MO's.

7. Select CI basis functions (see section 3.5).

8. Diagonalize Hamiltonian with the multi-configuration single and double excited configuration state functions (SOCI).

9. Obtain multiplets and corresponding eigenvectors with optimized coefficients for configuration state functions.

In the next chapter, we present the calculated results.

Chapter 4

Calculated Results

4.1 Introduction

In this chapter, the calculated multiplet energy levels of six lanthanide ions, Pr^{3+}, Pm^{3+}, Eu^{3+}, Tb^{3+}, Ho^{3+}, Tm^{3+} and a $(TmP_4)^{3+}$ cluster are presented. The relativistic effect on the multiplet structures is discussed with the use of the effective nuclear charge. For the purpose, the effective nuclear charges for rare earth ions are calculated by Dirac-Slater method. The effective nuclear charge is relevant to a spin-orbit constant as shown in eq. (3.6). The relationship between the obtained Z_{eff} and one-electron energy gap by solving Dirac-Slater equation is examined. Further, we show a suitable contraction of $4f$ basis functions of the trivalent ions. The suitable contracted $4f$ basis function gives the lowest energy and the obtained multiplet energy levels using them are more close to experimental results than the previous numerical calculations. Then SOCI calculation for $(TmP_4)^{3+}$ cluster is given in which the quantitative evaluation of the crystal field effect is done. Finally, we estimate the luminescent optical process by comparing optical experiments with CI results.

4.2 Free trivalent ions

Here, we show calculated results of the effective nuclear charge, Z_{eff}, by the two numerical methods as is explained in 3.2. The calculated multiplet terms of the trivalent lanthanide ions with two different Z_{eff} are compared with each other.

4.2.1 Numerical relativistic and non-relativistic calculations of effective nuclear charge Z_{eff}

In order to compare Z_{eff}'s derived by relativistic and non-relativistic equations, we solve Dirac-Slater (DS) and Xα Schrödinger (XS) equations for all the trivalent lanthanide group ions. We will show SOCI results only for the trivalent ions with even number electrons. It is difficult to perform CI calculations of odd number electrons because the total spin-quantum number is a half integer and the double point group theory is need to describe the formulation.

In Table 4.1 Z_{eff} values obtained by two methods are compared. The DS values are always smaller than the XS ones by about unity. This implies a shrinkage of the inner core orbitals due to the relativistic effect as explained in 3.2. In contrast, the $4f$ orbital expands from the inner space to outside. In Figs. 4.1 and 4.2 , the wavefunction $rR_{1s}(r)$ and $rR_{4f}(r)$ are plotted as functions of r for Tm^{3+}. It is clear that the DS (solid line) $4f$ wavefunction expands more outwards than the XS (dashed line) $4f$ wavefunction, while the DS $1s$ wavefunction is more localized than the Xα $1s$ wavefunction. The expectation values of r for

Table 4.1: Effective nuclear charge Z_{eff} for $4f$ orbitals of RE^{3+} ions obtained by numerical Xα Schrödinger(XS) and Dirac-Slater (DS) equations and with the use of eq. (3.7).

RE^{3+}	Z_{eff} (XS)	Z_{eff} (DS)
Ce^{3+}	31.56	30.82
Pr^{3+}	32.60	31.86
Nd^{3+}	33.61	32.87
Pm^{3+}	34.61	33.87
Sm^{3+}	35.59	34.85
Eu^{3+}	36.56	35.81
Gd^{3+}	37.52	36.77
Tb^{3+}	38.49	37.72
Dy^{3+}	39.45	38.66
Ho^{3+}	40.40	39.58
Er^{3+}	41.34	40.51
Tm^{3+}	42.25	41.42
Yb^{3+}	43.21	42.33

Tm^{3+} with the $4f$ radial wavefunctions are 0.744 and 0.721 for DS and XS methods, respectively.

Here we define the screened nuclear charge at the distance r by

$$Z_{\text{SC}}(r) = r^2 \frac{du_0(r)}{dr}. \tag{4.1}$$

The $Z_{\text{sc}}(r)$ presents the nuclear charge screened by the core electrons which exist in the inner space of the distance of r. On the other hand, the effective nuclear charge Z_{eff} is the expectation values of the screened nuclear charge Z_{sc} weighted by $4f$ radial functions. According to the classical Slater's rule, the effective nuclear charge for the $4f$ electron of a Tm^{3+} ion is given by 69 - 1 $\times$ 46 - 0.35 $\times$ 11 = 19.15 which is much smaller than the present value because the overlaps between $4f$

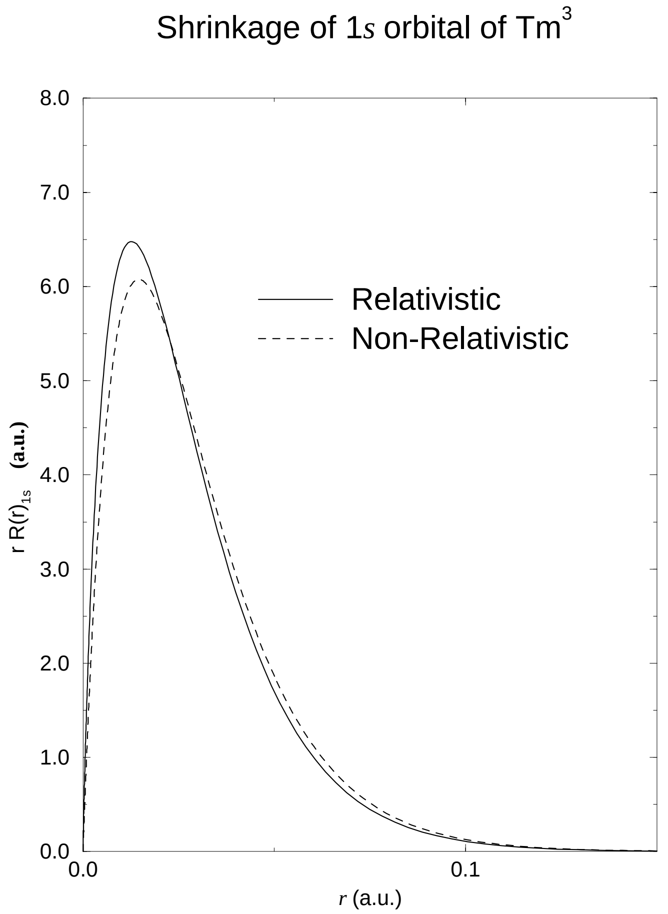

Figure 4.1: $rR_{1s}(r)$ calculated by DS (solid line) and XS (dashed line) equations in atomic unit, where $R_{1s}(r)$ is radial part of $1s$ orbital of Tm^{3+}.

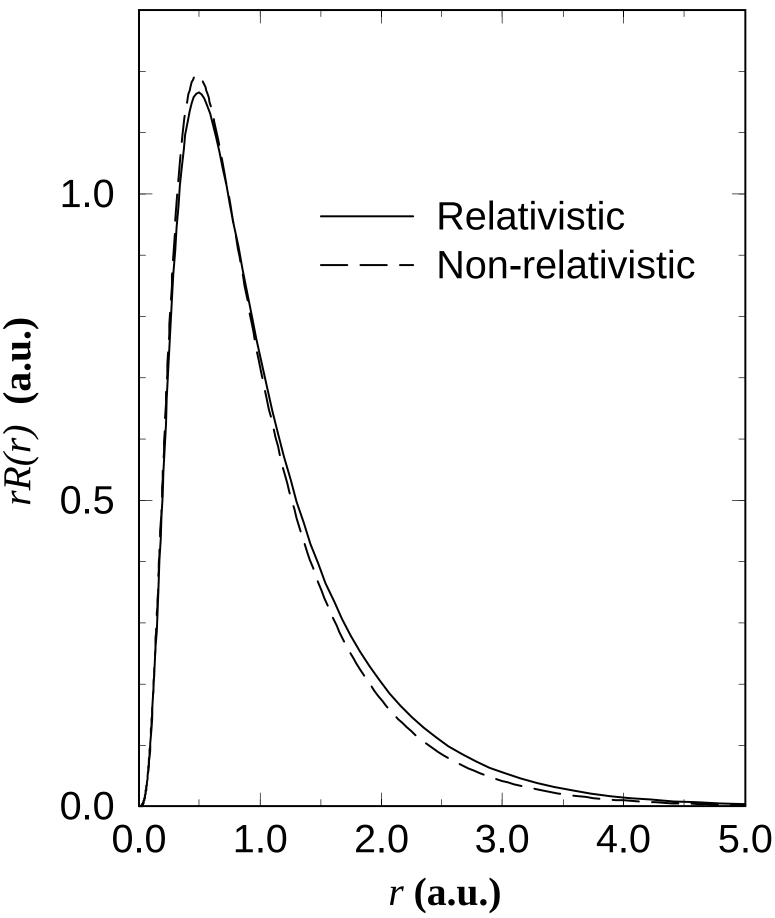

Figure 4.2: $rR_{4f}(r)$ calculated by DS (solid line) and XS (dashed line) equations in atomic unit, where $R_{4f}(r)$ is radial part of $4f$ orbitals of Tm^{3+}.

and the inner wavefunctions are not well considered in the Slater's rule. In Fig.4.3 the screened nuclear charge $Z_{\mathrm{SC}}(r)$ is plotted as a function of r (solid line) and also plotted the relativistic radial function $R_{4f}(r)$ (dashed line) for the $4f$ orbital of Tm^{3+}. The screened nuclear charge $Z_{\mathrm{SC}}(r)$ decreases from the bare nuclear charge of Tm^{3+} (69.00) to the ionic charge (3.00). The effective nuclear charge Z_{eff} in eq. (3.10) can be interpreted as a weighted average of $Z_{\mathrm{SC}}(r)$ with $R_{4\mathrm{f}}(r)$. The value of $Z_{\mathrm{SC}}(r)$ at the maximum value of $R_{4\mathrm{f}}(r)$ is almost 40 $\sim$ 45 which corresponds to Z_{eff} in Table 4.8.

We try to clarify the relativistic effect on the numerical basis sets obtained by the two methods. In Table 4.2 the expectation values of $\langle r^n \rangle$ $(n = 1, -1, -3)$ for the $4f$ orbitals obtained by DS and XS equations are listed and the reference data for neutral lanthanide atoms obtained by Dirac-Fock (DF) calculation [69] is also given for comparison. We can see $\langle r^1 \rangle$ that the expansion of $4f$ orbitals are within 0.03 $\sim$ 0.05 (a.u.) between DS and XS methods. It is not meaningful to compare DS and DF directly, since both results are given for the different charges of atoms and the different methods. However, we can see the expansion of $4f$ wavefunctions of neutral atoms relative to those of trivalent ions both by DS and DF methods. The ratios of expansion of (1) XS to DS and (2) DS to DF are in the same order. Thus, in order to include the relativistic effect in the Gaussian Basis sets for ions in the non-relativistic SCF-HF calculation, it is a good approximation to use the basis sets for non-relativistic neutral atoms. Here, it should be noted that the Gaussian Basis sets used in the present thesis are obtained by non-relativistic optimizations [62].

It is useful to show $\langle r^{-1} \rangle$ and $\langle r^{-3} \rangle$ in the table since these values

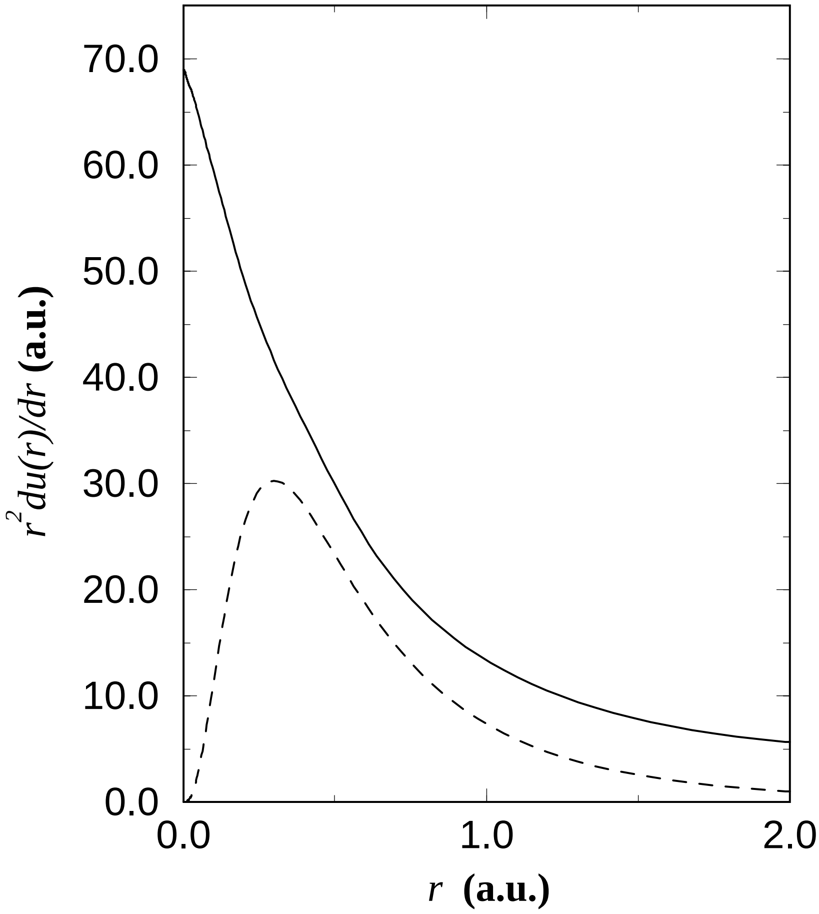

Figure 4.3: Screened nuclear charge $Z_{\mathrm{SC}}(r)$ (solid line) and the radial part of $4f$ orbital $R_{4f}(r)$ (magnified by ten times to the vertical axis, dashed line) by DS for Tm^{3+} are plotted. The value of $Z_{\mathrm{SC}}(r)$ at the maximum $R(r)$ corresponds to $40 \sim 45$. The nuclear charge Z_{eff} listed in Table 4.1 are obtained by a weighted average of $Z_{\mathrm{SC}}(r)$ with $R_{4f}(r)$.

are relevant to the matrix elements of physical properties. As is shown in Table 4.2, the expectation values $\langle r^{-1}\rangle$ by XS calculation are larger than by DS and DF calculations. It is because that $\langle r^{-1}\rangle$ emphasizes the behavior of wavefunctions near the origin and the expectation values become smaller due to the expansion of $4f$ orbitals. For all of the rare earth ions, the maximum expectation value $\langle r\rangle$ is 1.002 (XS), 1.053 (DS) in Ce^{3+} ($Z = 58$) and the minimum expectation value is 0.7029 (XS), 0.7345 (DS) in Yb^{3+} ($Z = 70$), respectively. On increasing the atomic number from Ce^{3+} up to Yb^{3+}, the expectation value $\langle r\rangle$ decreases monotonically, showing the well-known lanthanide contraction [53, 54]. As for $\langle r^{-3}\rangle$, SO operator has a form of r^{-3} and $\langle r^{-3}\rangle$ approximately represents the expectation value of the SO interactions. The expectation value $\langle r^{-3}\rangle$ of Yb^{3+} is about four times as large as that of Ce^{3+} by the three methods. This is consistent with the fact that spin-orbit separation in Yb^{3+} calculated using Dirac-Slater equation is about four times as large as that in Ce^{3+} (See Table 4.3).

One-electron $4f$ orbital energies obtained by the two numerical methods are listed in Table 4.3 in atomic unit. Since the Xα-Shrödinger equation is spin-dependent, one-electron energies split into two levels. The occupation of $4f$ electrons is fixed putting by them first for up-spins and then for down-spins according to Hund's rule. The energy splitting reflects the exchange-energy of $4f$ electrons.

The relativistic one-electron energy levels of the $4f$ orbital are split into κ=3 and κ=-4 due to spin-orbit interaction, where κ is the index of angular momentum. The spin-orbit splitting energy, denoted by $\Delta\epsilon_{\mathrm{so}}$, increases from 0.35 (in Ce^{3+}) to 1.41 (in Yb^{3+}) eV over the lanthanide ions. The increase in the splittings is consistent with the behavior of

Table 4.2: The expectation values for r^n with $4f$ orbitals of RE^{3+} ions. In addition to XS and DS, Dirac-Fock (DF) results for neutral RE atoms are listed for comparison.

	r^n	XS		DS		DF *)	
		up-spin	down-spin	$\kappa=-4$	κ=3	$\kappa=-4$	κ=3
Ce^{3+}	1	0.995	1.002	1.053	1.044	1.044	1.036
	−1	1.294	1.289	1.238	1.248	1.239	1.248
	−3	4.882	4.849	4.415	4.518	4.329	4.435
Pr^{3+}	1	0.952	0.966	1.007	0.998	1.100	1.088
	−1	1.350	1.339	1.293	1.304	1.216	1.228
	−3	5.491	5.418	4.984	5.106	4.348	4.478
Nd^{3+}	1	0.915	0.934	0.968	0.958	1.045	1.032
	−1	1.402	1.386	1.345	1.357	1.275	1.288
	−3	6.123	6.003	5.573	5.717	4.943	5.098
Pm^{3+}	1	0.882	0.906	0.933	0.923	0.999	0.986
	−1	1.453	1.431	1.394	1.407	1.330	1.345
	−3	6.781	6.607	6.185	6.353	5.552	5.736
Sm^{3+}	1	0.853	0.881	0.902	0.892	0.960	0.946
	−1	1.503	1.474	1.442	1.457	1.382	1.398
	−3	7.465	7.230	6.821	7.016	6.180	6.397
Eu^{3+}	1	0.826	0.859	0.874	0.864	0.925	0.912
	−1	1.551	1.516	1.489	1.505	1.431	1.449
	−3	8.179	7.874	7.484	7.708	6.830	7.083
Gd^{3+}	1	0.802	0.838	0.849	0.838	0.839	0.829
	−1	1.598	1.557	1.534	1.551	1.538	1.555
	−3	8.924	8.541	8.173	8.431	8.076	8.360
Tb^{3+}	1	0.781	0.810	0.825	0.814	0.868	0.853
	−1	1.643	1.608	1.579	1.597	1.525	1.547
	−3	9.695	9.347	8.892	9.187	8.204	8.545
Dy^{3+}	1	0.762	0.785	0.805	0.793	0.843	0.828
	−1	1.687	1.657	1.622	1.642	1.570	1.594
	−3	10.491	10.183	9.629	9.964	8.932	9.324
Ho^{3+}	1	0.744	0.762	0.785	0.773	0.820	0.804
	−1	1.729	1.706	1.664	1.686	1.614	1.640
	−3	11.312	11.051	10.394	10.774	9.688	10.137
Er^{3+}	1	0.728	0.741	0.767	0.755	0.800	0.783
	−1	1.771	1.753	1.705	1.729	1.658	1.686
	−3	12.157	11.950	11.190	11.619	10.473	10.986
Tm^{3+}	1	0.717	0.725	0.750	0.737	0.780	0.763
	−1	1.804	1.792	1.746	1.771	1.700	1.731
	−3	12.933	12.783	12.015	12.498	11.288	11.872
Yb^{3+}	1	0.699	0.703	0.734	0.721	0.762	0.744
	−1	1.851	1.845	1.786	1.813	1.742	1.775
	−3	13.940	13.863	12.871	13.414	12.134	12.797

*) Reference [69].

Table 4.3: $4f$ orbital one-electron energies by XS and DS equations (in atomic unit). The occupation number of $4f$ electrons is taken to follow the Hund's rule and the order of putting electrons is from up- to down- (XS) and from κ=−4 to 3 (DS).

RE^{3+}	XS		DS	
	up spin	down spin	κ=−4	κ=3
Ce^{3+}	−1.177	−1.146	−1.039	−1.052
Pr^{3+}	−1.235	−1.173	−1.081	−1.096
Nd^{3+}	−1.289	−1.193	−1.117	−1.134
Pm^{3+}	−1.337	−1.208	−1.149	−1.169
Sm^{3+}	−1.382	−1.219	−1.177	−1.200
Eu^{3+}	−1.423	−1.225	−1.202	−1.227
Gd^{3+}	−1.461	−1.228	−1.224	−1.252
Tb^{3+}	−1.480	−1.278	−1.243	−1.275
Dy^{3+}	−1.494	−1.325	−1.258	−1.293
Ho^{3+}	−1.504	−1.367	−1.270	−1.309
Er^{3+}	−1.509	−1.406	−1.280	−1.323
Tm^{3+}	−1.486	−1.417	−1.288	−1.336
Yb^{3+}	−1.513	−1.479	−1.294	−1.346

the expectation values of $\langle r^{-3}\rangle$.

In order to check the consistency, we calculate the following ratio,

$$\frac{2}{7}\frac{2}{\alpha^2}\frac{\Delta\epsilon_{\mathrm{so}}}{Z_{\mathrm{eff}}\langle r^{-3}\rangle}, \tag{4.2}$$

for each ion. The factor $\frac{2}{7}$ comes from the following formula [70],

$$\Delta\epsilon_{\mathrm{so}} = \frac{7}{2}\int_0^\infty \xi(r)R_{4f}(r)^2 r^2 dr, \quad \xi(r) = \frac{\alpha^2}{2}\frac{1}{r}\frac{du_0(r)}{dr}. \tag{4.3}$$

Here, one-electron spin-orbit splitting energies of $4f$ orbitals are denoted by $\Delta\epsilon_{\mathrm{so}}$. By the approximation of the core potential as is used in eq. (3.6), the one-electron spin-orbit splitting energy is given by

$$\frac{7}{2}\frac{\alpha^2}{2}\frac{Z_{\mathrm{eff}}}{r^3}. \tag{4.4}$$

Thus, the ratio of eq. (4.2) should be unity. In Fig. 4.4 the plotted data show the values calculated with eq. (4.2) over the rare earth ions. The ratios are always near unity, which shows that the method to derive an effective nuclear charge Z_{eff} is appropriate.

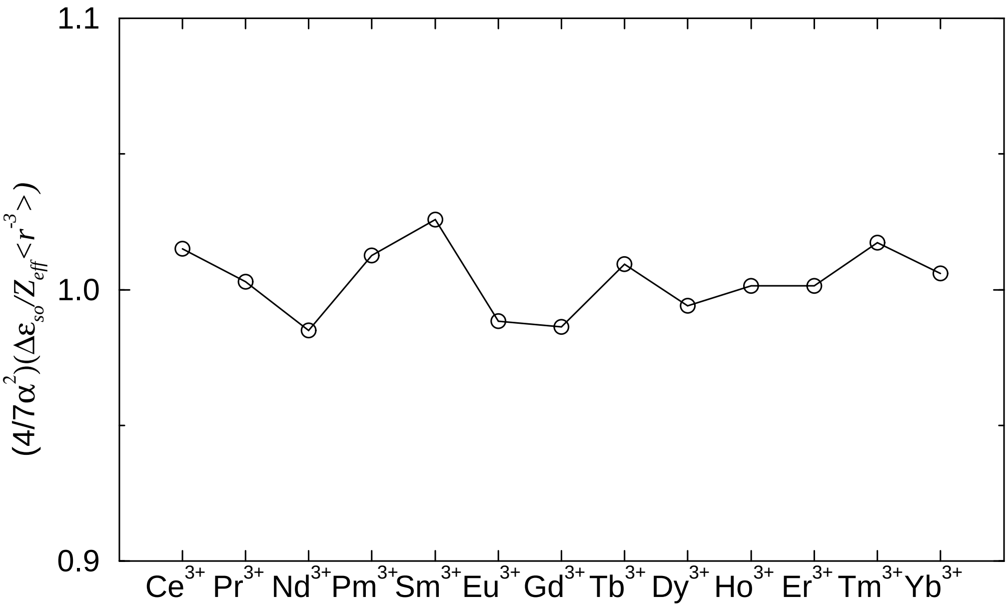

Figure 4.4: The ratios of $4f$ orbital energy gap $\Delta\epsilon_{\text{so}}$ by DS eq. to $\frac{7}{2}Z_{\text{eff}}$ $\langle r^{-3}\rangle$ for lanthanide ions.

4.3 SOCI calculation for trivalent ions

In this section, we will show the calculated multiplet terms for free ions. First, we show the multiplets for lanthanide ions with use of the two Z_{eff} values in 4.3.1. Next, we will propose the basis sets appropriate for the trivalent lanthanide ions in 4.3.2. The energy tolelances of all the calculated multiplets in this and text sections are in 10^{-4} a.u. $\simeq$ 22 cm^{-1} at most.

4.3.1 Multiplet terms calculated with Base I

The multiplet energy levels calculated by SOCI with the use of the two different effective nuclear charge Z_{eff} are tabulated in Table 4.4. As for basis sets, the Base I in Table 3.1 are adopted in this subsection. The values from the photoluminescence spectra for trivalent lanthanide ions in LaCl_3 compound and Dirac-Brait-Pauli-Hartree-Fock (DBPHF) values [29] are also shown in Table 4.4 for comparison. The total energies of SCF and CI calculations are listed in the table, too. Since Z_{eff} does not appear in the SCF calculation, the SCF total energy does not depend on the value of Z_{eff}. We can see that the relativistic Z_{eff} yields the multiplet energy levels more closely to the experimental results and the DBPHF results that contain all the relativistic corrections. The effect of Z_{eff} to the multiplet terms by the DS method is up to 300 cm^{-1}. The overall agreement is reasonably good despite a simple treatment for Z_{eff}.

There still exists descrepancy in the multiplet energies between the present results and the experimental data. As is shown in the next section, the remaining disappearement in the DBPHF method is mainly due to an unoptimized selection of the basis functions.

The configuration interactions are dominant within $4f$ electrons for the lower lying multiplets. In Table 4.5, the largest coefficients for a given spin S in the CI eigenvectors are listed . In the case of Pr^{3+}, the ground state ${}^3H_4$ is coupled with $S = 0$ of ${}^1G_4$. The ratio of the coefficients is $3 : 1$ in the same order. As for ${}^3H_5$, there is no multiplet with $S = 0$ in $J = 5$. Thus, there is no coupling between $S = 1$ and $S = 0$.

Table 4.4: Multiplet terms of RE^{3+} (in cm^{-1}) with the two $Z_{\rm eff}$'s. SCF and CI are in atomic unit.

RE	Terms	Multiplet energy			
		SOCI(XS)	SOCI(DS)	DBPHF [29]	Experiment [33]
Pr^{3+}	$^3H_6$	5961.7	5822.9	5286.	4330.9 - 4230.9 $^{a)}$
	$^3H_5$	2920.7	2849.4	2579.	2117.4 $^{a)}$
	$^3H_4$	0.0	0.0	0.0	0 - 96.05 $^{a)}$
	SCF	−8893.163625			
	CI	−8892.228710	−8892.228330		
Pm^{3+}	$^5I_8$	8779.2	8590.3	7979.	6525 - 6752 $^{b)}$
	$^5I_7$	6408.8	6261.6	5813.	4893 - 4933 $^{b)}$
	$^5I_6$	4126.2	4022.7	3729.	3170 - 3211 $^{b)}$
	$^5I_5$	1975.3	1914.6	1772.	1537 - 1620 $^{b)}$
	$^5I_4$	0.0	0.0	0.0	0.0 $^{b)}$
	SCF	−9623.975524			
	CI	−9624.225823	−9624.225239		
Eu^{3+}	$^7F_6$	6672.1	6539.1	6016.	4978 $^{c)}$
	$^7F_5$	5223.6	5103.1	4692.	3909.0 $^{c)}$
	$^7F_4$	3818.9	3726.6	3421.	2877.2 $^{c)}$
	$^7F_3$	2524.0	2452.7	2246.	1882.0 $^{c)}$
	$^7F_2$	1382.7	1342.9	1225.	1044.8 $^{c)}$
	$^7F_1$	485.0	485.9	441.	380.16 $^{c)}$
	$^7F_0$	0.0	0.0	0.0	0.0 $^{c)}$
	SCF	−10389.742459			
	CI	−10390.168586	−10390.165707		
Tb^{3+}	$^7F_0$	6820.0	6689.3	6578.	5615.93 $^{d)}$
	$^7F_1$	6553.6	6427.3	6316.	5386.90 $^{d)}$
	$^7F_2$	6007.1	5892.2	5783.	4939.24 $^{d)}$
	$^7F_3$	5179.7	5078.5	4974.	4263.27 $^{d)}$
	$^7F_4$	4001.1	3922.4	3831.	3270.63 $^{d)}$
	$^7F_5$	2475.7	2418.9	2350.	2018.79 $^{d)}$
	$^7F_6$	0.0	0.0	0.0	0.0 $^{d)}$
	SCF	−11191.222656			
	CI	−11191.636744	−11191.636172		
Ho^{3+}	$^5I_4$	15916.1	15619.8	15226.	13344. $^{e)}$
	$^5I_5$	13446.8	13191.2	12883.	11255. $^{e)}$
	$^5I_6$	10316.5	10103.7	9854.	8647. $^{e)}$
	$^5I_7$	6058.4	5919.6	5761.	5087. $^{e)}$
	$^5I_8$	0.0	0.0	0.0	0.0 $^{e)}$
	SCF	−12027.866088			
	CI	−12028.162259	−12028.161230		
Tm^{3+}	$^3H_6$	9667.4	9472.5	9308.	8285. $^{f)}$
	$^3H_5$	7133.9	7146.5	7085.	5795. $^{f)}$
	$^3H_4$	0.0	0.0	0.0	0.0 $^{f)}$
	SCF	−12900.619363			
	CI	−12900.868144	−12900.867239		

$^{a)}$ Reference [71, 72]. $^{b)}$ Reference [73, 74]. $^{c)}$ Reference [75]. $^{d)}$ Reference [76]. $^{e)}$ Reference [77]. $^{f)}$ Reference [78].

Although we use the symbol $^{2S+1}L_J$ for each multiplet, different S are mixed in the state because of spin-orbit interaction, in which only J is the same in the coupled multiplets. For the other lanthanide ions, the spin coupling between S and $S+1$ are not so large as is shown in Table 4.5. The only exceptions are the ground state of Pr^{3+} and the first excited state ($^3H_4$) of Tm^{3+}. The reason why we get a large mixing is that the excited multiplets with the same J is lying near the ground state.

In Table 4.6, we show the splitting of ^{2S+1}L multiplet terms without considering SO interactions to see the magnitude of Coulomb splitting. These result can be easily obtained by putting Z_{eff}=0. As shown in Table 4.6, the Coulomb interaction between ^3H and ^3F is $\sim$ 8300 cm^{-1}, ($\sim$ 1 eV) and that between ^3F and ^3P is $\sim$ 30000 cm^{-1}, ($\sim$ 3.7 eV). Since the energy difference between ^3H and ^3F states is in the same order as that of SO interaction between $^3H_4$ or $^3H_5$ and $^3H_6$ as shown in Table 4.7, the SO coupling between ^3H and ^3F is significantly important for the present case. In Table 4.7, it is obvious that the CI expansions using the MO's obtained for the average-state give reasonable multiplet energies. The multiplets of a Tm^{3+} ion are illustrated in Fig. 4.5 (a) and (b). In Fig. 4.5 (a) we show the multiplets of a Tm^{3+} ion neglecting SO interaction and in Fig. 4.5 (b) SO splittings for ^3H state. In order to obtain SO splitting of ^3F and ^3G states it is necessary to calculate much higher multiplets though SO splittings of those states are not shown in the Fig. 4.5 (b).

The main excitation, which is taken into account in SOCI, consists of configuration interactions between $4f$ electrons within $4f$ orbitals. In the eigenvector of the multiplet terms, the coefficients for the single or double excitations are less than 0.02. The observed luminescence spectra are caused by excitations within $4f$ orbitals, that is, a $4f^n \rightarrow 4f^n$ type transition and thus, the CI results are in good agreement with the experiences.

In Table 4.7, the SO splittings for the ^3H state of a Tm^{3+} ion are shown with different open-shell energy coefficients for ^3H and averaged-state. It is noted that Z_{eff} for Tm^{3+} is set to 41 in Table 4.7 and Fig. 4.5. Though the difference of the total energies between the two states can be distinguished in the SCF calculation, it would be neglegible in the CI calculation. This shows that the ground state of rare earth ions can be represented by the many electronic state and the one-electron orbital is not sufficient for coupled states by the spin-orbit interaction.

The multiplet energies of Tm^{3+} for various Z_{eff} are listed in Table 4.8. As Z_{eff} value decreases from 69 to 41 in Eq.(3.20), the second excited state decreases, too, while the first excited state does not change much. The reason why the first excited state $^3H_4$ is less sensitive to Z_{eff} value is that the second-order perturbation of SO interactions between $^3H_4$ and $^3F_4$ states cancels the first-order perturbation. On the other hand there is no '$J = 5$' multiplet state near the ^3H state and the energy position of the $^3H_5$ state is sensitive to a change of SO interaction.

4.3.2 Multiplet terms calculated with Base II

In this section, we present the results with use of Base II in which we use contracted $4f$ and uncontracted $4d$ orbitals.

The present SOCI results with use of Z_{eff} by DS are tabulated in

Table 4.5: The largest coefficients of the CSF's for different spins in CI eigenvectors of the multiplet terms.

RE^{3+}	Terms	Spin mixing in CI eigen vector	
		$S=1$	$S=0$
	$^3H_6$	0.410057	0.035855
Pr^{3+}	$^3H_5$	0.564157	0
	$^3H_4$	-0.459193	-0.155313
		$S=2$	$S=1$
	$^5I_8$	-0.357333	-0.041700
	$^5I_7$	-0.387926	0.037991
Pm^{3+}	$^5I_6$	0.422967	-0.029802
	$^5I_5$	0.332879	0.029156
	$^5I_4$	0.337902	-0.031615
		$S=3$	$S=2$
	$^7F_6$	-0.482572	0.048929
	$^7F_5$	0.497103	0.038334
	$^7F_4$	-0.681388	-0.033980
Eu^{3+}	$^7F_3$	0.382865	0.043014
	$^7F_2$	0.509054	0.041907
	$^7F_1$	-0.535154	0.049068
	$^7F_0$	-0.36479	0.041414
		$S=3$	$S=2$
	$^7F_0$	0.367708	0.044912
	$^7F_1$	0.450542	0.053138
	$^7F_2$	-0.483669	0.044848
Tb^{3+}	$^7F_3$	-0.398412	-0.050864
	$^7F_4$	-0.617470	0.041511
	$^7F_5$	-0.559836	-0.044971
	$^7F_6$	0.627055	0.053683
		$S=2$	$S=1$
	$^5I_4$	-0.337356	0.061197
	$^5I_5$	-0.405431	-0.082786
Ho^{3+}	$^5I_6$	-0.396009	0.070155
	$^5I_7$	0.408792	0.050804
	$^5I_8$	0.424957	-0.062322
		$S=1$	$S=0$
	$^3H_5$	-0.470327	0
Tm^{3+}	$^3H_4$	-0.372906	-0.444223
	$^3H_6$	-0.558192	0.068145

Table 4.6: Multiplet terms of Tm^{3+} ion without SO coupling. (in cm^{-1} unit).

multiplet terms	energy
^3P	38711.
^3F	8362.
^3H	0.

Table 4.7: The multiplet energy, SCF and CI total energies of Tm^{3+} ion using the different open-shell energy coefficients for ^3H and average state. Multiplet energies are in cm^{-1} and total energies are in atomic unit.

	^3H state	average state
$^3H_5$	9373.	9372.
$^3H_4$	7153.	7153.
$^3H_6$	0.	0.
SCF (a.u.)	−12900.7265	−12900.6193
CI (a.u.)	−12900.8670	−12900.8668

Table 4.8: Multiplet energies of Tm^{3+} for various Z_{eff} (in cm^{-1} unit).

Z_{eff}	69	60	50	41	experiment[12]	DBPHF[29]
$^3H_5$	16051.	13877.	11496.	9373.	8100.	9308.
$^3H_4$	6639.	6809.	6998.	7153.	none	7085.
$^3H_6$	0.	0.	0.	0.	0.	0.

Figure 4.5: Multiplet energy levels of (a)a Tm^{3+} ion without SO interaction, (b)Tm^{3+} with SO interaction and (c)a $(TmP_4)^{3+}$ cluster

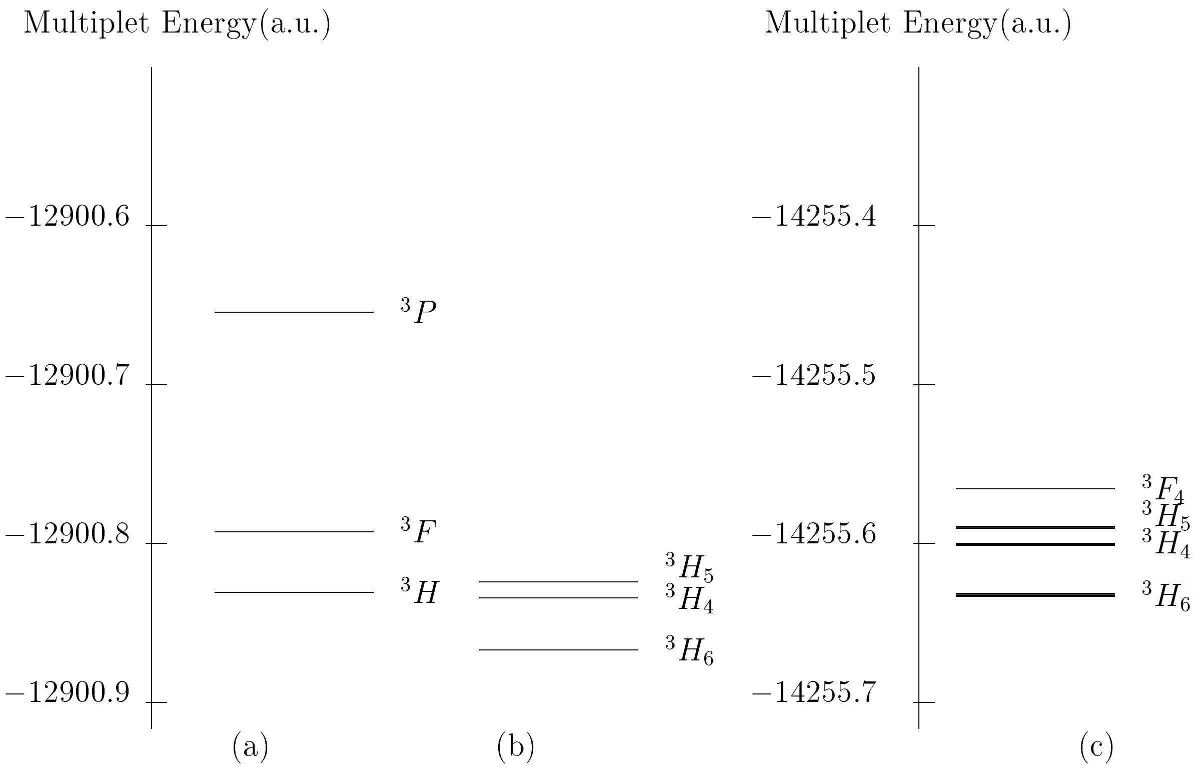

Table 4.9. The values from Dirac-Breit-Pauli-Hartree-Fock (DBPHF) calculations [29] and the photoluminescence spectra for trivalent lanthanide ions doped in $LaCl_3$ compounds [33] are also shown in Table 4.9 for comparison. We can see that the present SOCI method can yield multiplet energy levels closer to the experimental results than the DBPHF values relative to the result of Base I. These results show that the expansions of $4f$ orbitals, which are not included in the previous calculations [59], are important in the SOCI calculations. A difference of $4f$ orbitals between Base I and Base II is the contraction of $4f$ orbitals. In Base I, the outermost $4f$ orbital is not contracted, while all of the primitive sets of $4f$ orbitals are completely contracted in Base II. Thus, the $4f$ orbitals of Base I are more flexible than Base II which may be useful for ions. In fact, the ionic $4f$ orbitals are more localized than the neutral ones in SCF calculations. In this sense, the Base II can be considered as "expanded $4f$ orbitals".

In the present SCF and SOCI calculations, however, the single-zeta basis function for $4f$ orbitals (SZ-$4f$) yield lower CI total energies because the Coulomb energies between the $4f$ electrons are reduced in the expanded orbitals. ($ECI_{(SZ-4f)} = -12901.0476$ and $ECI_{(DZ-4f)} = -12900.8672$) The obtained multiplet energies with the SZ-$4f$ orbitals go down by $40 \sim 630$ (cm^{-1}) for ions. The reason why we get better results than the previous ones with use of double-zeta $4f$ basis functions is that the contracted $4f$ GTO's, which expand to outwards for ions, lead to less SO splittings of the multiplet energies. The expanded $4f$ orbitals will become better by including the relativistic term in the SCF-CI method. This situation is already realized by DS calculation as shown in Fig. 4.2.

Table 4.9: Multiplet terms of RE^{3+} (in cm^{-1}) with use of Base II the $Z_{\rm eff}$ obtained by DS.

RE^{3+} Ions.	$^{2S+1}L_J$	Multiplet Energy (cm^{-1})		
		Present Results	DBPHF [29]	Experiment [33]
Pr^{3+}	$^3H_6$	5188.9	5286.	4330.9 - 4230.9 a)
	$^3H_5$	2538.7	2579.	2117.4 a)
	$^3H_4$	0.0	0.	0 - 96.05 a)
Pm^{3+}	$^5I_8$	7775.5	7979.	6525 - 6752 b)
	$^5I_7$	5675.1	5813.	4893 - 4933 b)
	$^5I_6$	3647.3	3729.	3170 - 3211 b)
	$^5I_5$	1736.3	1772.	1537 - 1620 b)
	$^5I_4$	0.0	0.	0.0 b)
Eu^{3+}	$^7F_6$	5971.2	6016.	4978 c)
	$^7F_5$	4674.5	4692.	3909.0 c)
	$^7F_4$	3422.6	3421.	2877.2 c)
	$^7F_3$	2257.3	2246.	1882.0 c)
	$^7F_2$	1238.1	1225.	1044.8 c)
	$^7F_1$	448.4	441.	380.16 c)
	$^7F_0$	0.0	0.	0.0 c)
Tb^{3+}	$^7F_4$	3738.6	3831.	3270.63 d)
	$^7F_5$	2297.5	2350.	2018.79 d)
	$^7F_6$	0.0	0.	0.0 d)
Ho^{3+}	$^5I_7$	5557.8	5761.	5087. e)
	$^5I_8$	0.0	0.	0.0 e)
Tm^{3+}	$^3H_5$	8958.5	9308.	8285. f)
	$^3H_4$	6851.3	7085.	5795. f)
	$^3H_6$	0.0	0.	0.0 f)

Experimental observations are summarized in a figure of ref. [33]. Listed numerical data of experiments are referred to the following papers, respectively. *a)* Reference [71, 72]. *b)* Reference [73, 74]. *c)* Reference [75]. *d)* Reference [76]. *e)* Reference [77]. *f)* Reference [78].

The contribution of the excitations of $4f$ electrons to $5d$ and $6s$ orbitals to CI expansions are small. The absolute values of the coefficients of the configuration state functions for the excitations are less than 1 %. Thus, we can say that the photoluminescent excitations of the $4f$ electrons are due to the intra-transitions in the $4f$ orbitals.

Let us explain the comparison between the present result and the other *ab initio* calculation [28]. In that paper, Visser *et al.* calculated the multiplet terms of a free Eu^{3+} ion and a cluster containing the ion by Dirac-Fock complete open-shell CI (COSCI) method. The calculated multiplets are listed in Table 2.5. The obtained values of the multiplet terms for a free Eu^{3+} ion, from the ground state ${}^7F_0$ up to ${}^7F_6$, are of 0, 375, 1058, 1962, 3022, 4129, 5430 cm^{-1}. They show better agreement with the experimental results than the present results. The reason why they got better results in CI calculations may come from that (1) the relativistic *ab initio* (Fock-Dirac) is adopted in a SCF calculation and that (2) the obtained Gaussian basis sets are well optimized. As for (1), it is reasonable to get better SCF vectors by the fully relativistic calculations. Since the dimensions of CI expansions by their method is in the same order as our calculation, we suppose that the reason of (1) is important.. In fact, the total energy by the Fock-Dirac CI is -10421.64489 a.u. which is lower than that of the present result -10390.434745 a.u. Though this large difference of the CI total energy clearly comes from the difference of the Hamiltonian, the obtained multiplet energies in the present method make no large difference. It is because that the multiplet energy is less sensitive to the difference of the total energy. Thus, the present method is reasonable in the sense that the relative energy gives a good agreement with experimental results.

4.4 $(TmP_4)^{3+}$ cluster

4.4.1 Introduction

In section 4.3 , we confirmed that a single lanthanide ion was a reasonable model for the present system because the multiplet energy levels caused by SO interaction come mainly from $4f$-$4f$ interactions. On the other hand, we also have interests in the lanthanide ions in semiconductors as impurities and the split multiplet terms by surrounding semiconductor atoms in order to clarify the structure multiplets of $4f$ electrons. The nature of chemical bonding is significant as fundamental information of compounds. In this section, we describe one-electron energy levels and the dependence of chemical bonding on the host semiconductor atoms for a $(TmP_4)^{3+}$ clusters with Base III in Table 3.1. Next, we show the multiplet structures of Tm^{3+} ion surrounded by four P atoms. Finally, we suggest the type of transitions for $4f$ electrons.

4.4.2 SCF calculations

First, we discuss the character of one-electron MO's of a cluster. The SCF one-electron orbital energy of a $(TmP_4)^{3+}$ cluster is shown in Fig. 4.6 in which $5s$, $5p$ and $4f$ MO's of Tm^{3+} and $3s$, $3p$ MO's of P are shown. $3p$ MO's of P atoms are the highest occupied molecular orbital (HOMO) and Tm^{3+} $4f$ MO's are specified to be partially occupied. It is noted that the occupation number of $4f$ electron is fixed to be $\frac{12}{7}$.

Because of weak covalent bonding between Tm^{3+} and P, the atomic nature of a Tm^{3+} ion remains in the molecular orbitals (MO's). In fact, the components of P atoms are no more than 1 % in the valence MO's for a Tm^{3+} ion. We show the valence MO's as bellow,

$$\Phi_{\mathrm{Tm}\ \mathrm{MO}}^{\ 4f} = 0.4\varphi_{\mathrm{Tm}}^{\ 4f} - 0.037\varphi_{\mathrm{Tm}}^{\ 5s} + 0.035\varphi_{\mathrm{P}}^{\ 3s} + 0.046\varphi_{\mathrm{P}}^{\ 3p}, \tag{4.5}$$

and

$$\Phi_{\mathrm{P}\ \mathrm{MO}}^{\ 3p} = -0.15\varphi_{\mathrm{Tm}}^{\ 4s} - 0.33\varphi_{\mathrm{Tm}}^{\ 5s} - 0.06\varphi_{\mathrm{Tm}}^{\ 4f} + 0.14\varphi_{\mathrm{P}}^{\ 3s} - 0.10\varphi_{\mathrm{P}}^{\ 2p} + 0.38\varphi_{\mathrm{P}}^{\ 3p}, \tag{4.6}$$

where, φ's represent the component of the atomic orbitals of Tm^{3+} or P.

Figure 4.6: One-electron energy levels of a $(TmP_4)^{3+}$ cluster. Specified atomic characters are mainly included in the MO's.

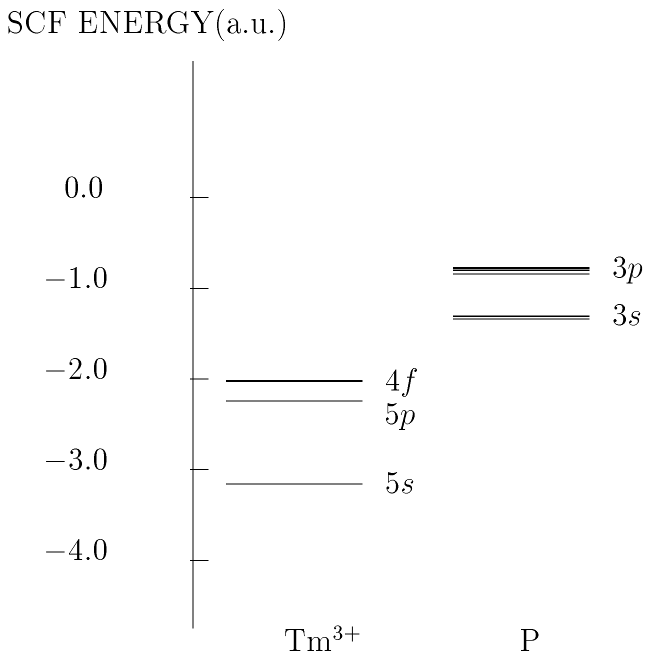

In eq. (4.5), we can say that $4f$ orbitals keep the atomic nature in the cluster. The components of other atomic orbitals are bellow 10

% of the $4f$ component. In eq. (4.6), the valence MO's for ligand P atoms have weak covalency with $4f$ orbitals. We may call Tm^{3+} MO or P MO even for a $(TmP_4)^{3+}$ cluster.

4.4.3 Multiplet terms

In Fig 4.5, the basic view of hierarchic interactions of the multiplets of (a) Coulomb interaction, (b) spin-orbit interaction and (c) crystal field effects are shown for Tm^{3+} ion. The detail of the crystal field splitting is shown in Fig. 4.7. From Fig. 4.5 the contribution of the ligand atoms to $4f$-multiplet energies is shown to be very small relative to Coulomb and SO interactions. The magnitude of the splitting for $4f$ MO's by ligand atoms is $\sim$ 0.29 eV.

The multiplet energy levels of Tm^{3+} are splitted by the crystal field into the irreducible representations of T_d symmetry. For the ground state ${}^3H_6$,

$$^3H_6 \to A_1 + A_2 + E + T_1 + 2T_2.$$

The decompositions of the lowest three multiplet terms $4f^{12}$ into T_d irreducible representations are listed in Table 4.10.

Table 4.10: Decompositions of the multiplet terms of $4f^{12}$ into T_d symmetry.

multiplet terms		T_d
$^3H_5$	$\Longrightarrow$	$E + 2T_1 + T_2$
$^3H_4$	$\Longrightarrow$	$A_1 + E + T_1 + T_2$
$^3H_6$	$\Longrightarrow$	$A_1 + A_2 + E + T_1 + 2T_2$

To our knowledge only one paper was reported [12] about the optical measurement of luminescence of Tm^{3+} in InP and the observed spectrum at 8100 cm^{-1} corresponds to the transition $^3H_5 \rightarrow {}^3H_6$.

The present results of multiplet energy splitting in $(\mathrm{TmP}_4)^{3+}$ cluster are shown in Fig. 4.7 and Table 4.11. The results in Table 4.11 do not follow the irreducible representations of T_d. This artificial structures are caused by the $3p$ MO's of P atoms which are open-shell structures. The localized $4f$ orbitals does not hybridize with the ligand MO's as is seen in eq. (4.6). Especially, the bonding 3p MO's are unstable in the present SCF iterations. In order to obtain convergence in SCF calculation, we adopted the bonding 3p MO's as unoccupied virtual orbitals. This caused the artificial crystal field splitting patterns. We should improve the one-electron atomic orbitals of the $4f$ and the $3p$ orbitals.

In the present case, the crystal field effects are ~ 0.05 eV ($\sim 417.$ cm^{-1}) for $^3H_6$ and ~ 0.036 eV ($\sim 287.$ cm^{-1}) for $^3H_4$ and ~ 0.032 eV ($\sim 276.$ cm^{-1}) for $^3H_5$.

The mixture of spin multiplicities between $S = 1$ and $S = 0$ for a $(\mathrm{TmP}_4)^{3+}$ cluster are similar to the case of a Tm^{3+} ion. Actually, the coefficients are (1) ~ 0.5 ($S = 1$) and ~ 0.06 ($S = 0$) for $^3H_6$, (2) $\sim$ 0.4 ($S = 1$) and ~ 0.4 ($S = 0$) for $^3H_4$ and (3) ~ 0.5 ($S = 1$) and 0 ($S = 0$) for $^3H_5$.

The dominant CSF's coefficients ($0.1 \sim 0.6$) are those for configurations consisting of only $4f$ MO's. On the other hand the magnitudes of CI coefficients of single and double excitations to external MO's are very small (less than 0.02). This shows that the excitation to outer orbitals from $4f$ is not so important and the main CSF's of a $(\mathrm{TmP}_4)^{3+}$ cluster consist of the configuration interactions between $4f$ electrons. This situation is already seen in the case of ions.

Figure 4.7: Crystal field splitting of ^3H of a $(TmP_4)^{3+}$ cluster.

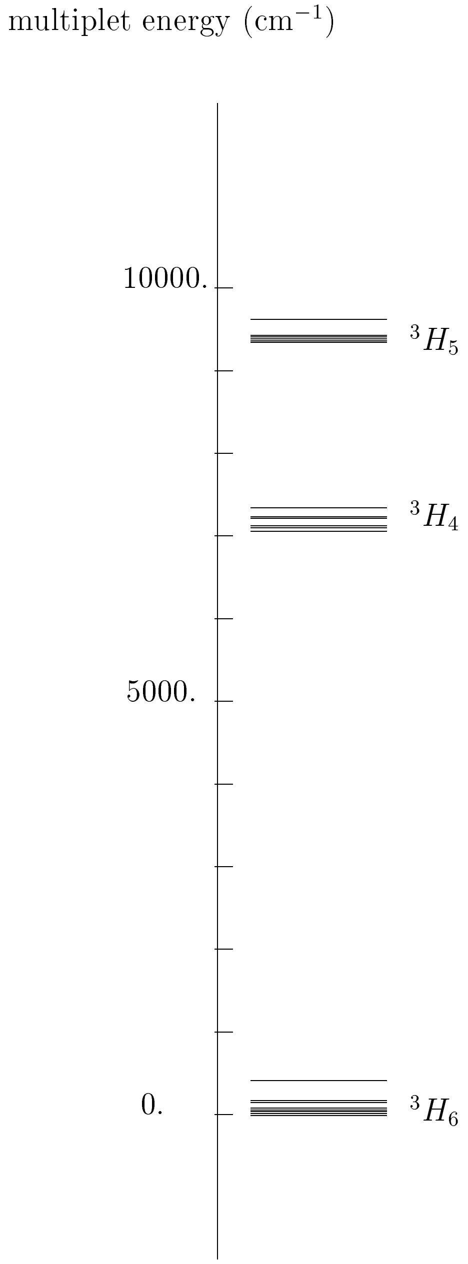

Table 4.11: Multiplet energies for $^3H_6$, $^3H_4$ and $^3H_5$ of $(\mathrm{TmP}_4)^{3+}$ cluster.

multiplet terms	energy (cm^{-1})
$^3H_5$	9625
	9625
	9438
	9416
	9416
	9394
	9394
	9372
	9372
	9372
	9350
$^3H_4$	7353
	7243
	7243
	7221
	7221
	7133
	7133
	7111
	7067
$^3H_6$	417.0
	417.0
	175.6
	153.6
	153.6
	87.8
	65.8
	65.8
	43.9
	43.9
	21.9
	21.9
	0.0

The dominant configurations for $^3H_5$ are the high spin state of $S = 1$ and are the same as $^3H_6$. Thus, although the transition is exactly determined by the selection rule of δJ=1 in the case of a free ion, the spin multiplicity of these two multiplets endures the electric dipole transition corresponding to $^3H_5 \rightarrow {}^3H_6$ even in the case of a cluster, that is consistent with the experimental observation. On the other hand, $^3H_4$ states contain a low spin ($S = 0$) state as is mentioned above. Thus, the transitions of $^3H_5 \rightarrow {}^3H_6$ are supposed. This low spin state is mixed with the high spin state of $^1G_4$ by the large intermediate coupling. The singlet $S = 0$ spin states also exist in $^3H_6$ but the coefficients of $S = 0$ CSF's are much smaller than those of $S = 1$ CSF's ($\sim 10\%$). It is because the possible intermediate coupling of $^3H_6$ with $S = 0$ is $^1I_6$, but the multiplet energy of $^1I_6$ is much higher. As for $^3H_5$ state, because there is no $J = 5$ multiplet terms with $S = 0$, the spin states are only those of $S = 1$ in the CSF's. These spin multiplicities of CSF's are similar to those of single Tm^{3+} ion in the present calculation. In this way, the intermediate coupling that can be obtained by *ab initio* SOCI calculation is essential to know the transition probability between the excited states and the ground states.

Chapter 5

Conclusion

In summary, we performed spin-orbit *ab initio* calculations for trivalent lanthanide ions with even number electrons and for a $(TmP_4)^{3+}$ cluster.

The multiplet energy levels for six lanthanide ions, Pr^{3+}, Pm^{3+}, Eu^{3+}, Tb^{3+}, Ho^{3+} and Tm^{3+}, and for a $(TmP_4)^{3+}$ cluster were calculated by the non-relativistic SCF-HF calculations and the consequent SOCI method in which the one-body spin-orbit interaction Hamiltonian is taken into account.

In order to consider the open-shell structures of $4f$ electrons, open-shell energy coefficients are calculated using averaged state wavefunctions.

A relativistic effect for the inner core is included in the spin-orbit Hamiltonian with the use of effective nuclear charges which are obtained by solving the atomic Dirac-Slater equation. The relativistic effect on the expansions of $4f$ wavefunctions is well described by reducing of the effective nuclear charges and adopting the basis functions for neutral lanthanide atoms. We find that the relativistic corrections for the $4f$ orbitals are important for the multiplet energies.

The crystal field effect is included in a calculation for a $(TmP_4)^{3+}$ cluster. The one-electron molecular orbitals keep the atomic nature for a Tm^{3+} ion. The multiplet terms are splitted by the crystal field effect much more weakly than by the Coulomb and spin-orbit effects.

Acknowledgements

The author would like to express his gratitude to Professor Riichiro Saito for his earnest and kind guidance through the present doctoral research. He also thanks Professor Tadamasa Kimura for valuable discussions and his encouragement. He wishes to thank Professor Satoshi Yabushita for his valuable advices for the theoretical methods not only on the library program COLMBS but also on the basic idea of quantum chemistry. He thanks Dr. Takashi Nakayama his providing a computational program for the Dirac-Slater method. He is also much pleased with the discussions with Professor Yugo and all the members of the research group under Professor T. Kimura and Professor R. Saito.

The computations were performed by the HITAC S-820 computer systems at the Institute of Molecular Science, Okazaki, Japan.

Bibliography

[1] V. A. Kasatkin, F. P. Kesamanly, V. G. Makarenko, V. F. Masterov, and B. E. Samorukov. *Sov. Phys. Semicond.*, 14:1092, 1980.

[2] K. Takahei, A. Taguchi, H. Nakagome, K. Uwai, and P. S. Whitney. *J. Appl. Phys.*, 66:4941, 1989.

[3] Y. S. Tang, K. C. Heasman, W. P. Gillin, and B. J. Sealy. *Appl. Phys. Lett.*, 55:432, 1989.

[4] W. Korber and A. Hangleiter. *Appl. Phys. Lett.*, 52:114, 1988.

[5] G. Aszodi, J. Weber, Ch. Uihlein, L. Pu-lin, H. Ennen, U. Kaufmann, J. Schneider, and J. Windscheif. *Phys. Rev.*, B31:7767, 1985.

[6] H. Ennen, J. Wagner, H. D. Muller, and R. S. Smith. *J. Appl. Phys.*, 61:4877, 1987.

[7] A. Kozanecki and R. Groetzschel. *J. Appl. Phys.*, 68:517, 1990.

[8] H. D. Muller and J. Schneider. *Appl. Phys. Lett.*, 57:1, 1990.

[9] H. Issiki, R. Saito, and T. Kimura. *J. Appl. Phys.*, 70:6993, 1991.

[10] H. Issiki, H. Kobayashi, S. Yugo, T. Kimura, and T. Ikoma. *Appl. Phys. Lett.*, 58:484, 1991.

[11] H. Issiki, H. Kobayashi, S. Yugo, T. Kimura, and T. Ikoma. *Jpn. J. Appl. Phys.*, 30:225, 1991.

[12] G. S. Pomrenke, E.Silkowski, J.E. Colon, D.J. Topp, Y.K. Yeo, and R.L. Hengehold. *J. Appl. Phys.*, 71:1919, 1992.

[13] H. Adachi, M. Tsukada, and C. Satoko. *J. Phys. Soc. Jpn.*, 45:875, 1978.

[14] M. V. Ryzhkov, V. A. Gubanov, Yu. A. Teterin, and A. S. Baev. *Z. Phys. B.*, 59:1, 1985.

[15] M. V. Ryzhkov, V. A. Gubanov, Yu. A. Teterin, and A. S. Baev. *Z. Phys. B.*, 59:7, 1985.

[16] Xinwei Zhao, K. Hirakawa, and T. Ikoma. In *Gallium Arsenide and Related Conpounds 1988*. Inst. Phys. Conf., 1989.

[17] Xinwei Zhao, K. Hirakawa, and T. Ikoma. *Appl. Phys. Lett.*, 54:712, 1989.

[18] F. Bautien, E. Bauser, and J. Weber. *J. Appl. Phys.*, 61:2803, 1987.

[19] A. Kozanecki and R. Groetzschel. *J. Appl. Phys.*, 69:1300, 1991.

[20] H. Ennen, G. Pomrenke, and A. Axmann. *J. Appl. Phys.*, 57:2182, 1985.

[21] K. Uwai, H. Nakagome, and K. Takahei. *Appl. Phys. Lett.*, 51:1010, 1987.

[22] K. Uwai, H. Nakagome, and K. Takahei. *Appl. Phys. Lett.*, 50:977, 1987.

[23] M. Taniguchi, H. Nakagome, and K. Takahei. *Appl. Phys. Lett.*, 58:2930, 1991.

[24] J. D. Ralston, H. Ennen, P. Wennekers, P. Hiesinger, N. Herres, J. Schneider, H. D. Muller, W. Rothemund, F. Fuchs, J. Schmalzlin, and K. Thonke. *J. Electr. Mater.*, 19:555, 1990.

[25] B. R. Judd. *Phys. Rev.*, 127:750, 1962.

[26] G. S. Ofelt. *J. Chem. Phys.*, 37:511, 1962.

[27] L. A. Hemstreet. *Mater. Sci. Forum*, 10-12:85, 1986.

[28] O. Visser, L. Visscher, P. J. C. Aerts, and W. C. Nieuwpoort. *J. Chem. Phys.*, 96:2910, 1992.

[29] S. Fraga, J. Harwowski, and K.M.S. Saxena. *Handbook of Atomic Data*. Elsevier, 1976.

[30] R. Shepard, I. Shavitt, R. M. Pitzer, D. C. Comeau, M. Pepper, H. Lischka, P. G. Szalay, R. Ahlrichs, F. B. Brown, and J. G. Zhao. *Int. J. Quantum. Chem. Symp.*, 22:149, 1988.

[31] K. Morokuma, K. Yamashita, and S. Yabushita. In A. Lagana, editor, *Supercomputer algorithms for reactivity, dynamics and kinetics of small molecules p. 37.* Kluwer, Dordrecht, 1989.

[32] H. G. Kahle. *Z. Phys.*, 161:486, 1961.

[33] G. H. Dieke and H. M. Crosswhite. *Appl. Opt.*, 2:675, 1963.

[34] D. D. Koelling, D. E. Ellis, and Rodney J. Bartlett. *J. Chem. Phys.*, 65:3331, 1976.

[35] M. Boring and J. H. Wood. *J. Chem. Phys.*, 71:32, 1979.

[36] R. Saito and T. Kimura. *Phys. Rev.*, B46:1423, 7.1992.

[37] P. Jeffrey Hay. *J. Chem. Phys.*, 79:5469, 11.1983.

[38] L. R. Kahn, P. J. Hay, and R. D. Cowan. *J. Chem. Phys.*, 68:2386, 1978.

[39] M. Dolg, H. Stoll, and H. Preuss. *J. Chem. Phys.*, 90:1730, 1989.

[40] V. Bonifacic and S. Huzinaga. *J. Chem. Phys.*, 60:2779, 1974.

[41] L. R. Kahn and W. A. Goddard III. *Chem. Phys. Lett.*, 2:667, 1968.

[42] R. M. Pizter and N. W. Winter. *J. Chem. Phys.*, 92:3061, 1988.

[43] W. C. Martin, R. Zalubas, and L. Hagan. *Atomic energy levels-The rare earth elements, Natl. Stand. Ref. Data Ser., Ntl. Bur. Stand. No.60.* U.S. GPO, Washington, D.C., 1978.

[44] I. P. Grant, B. J. McKenzie, P. H. Norrington, D. F. Mayers, and N. C. Pyper. *Comput. Phys. Commun.*, 21:1980, 1980.

[45] C. F. Fischer. *Comput. Phys. Commun.*, 1:151, 1969.

[46] M. Dolg. *modified version of the program MCHF77.*

[47] H. A. Bethe and E. E. Salpeter. *Quantum Mechanics of One- and Two-Electron Atoms.* Springer, Berlin, 1957.

[48] W. G. Richards, H. P. Trivedi, and D. L. Cooper. *Spin-Orbit Coupling in Molecules.* Oxford University, Clarendon, London, 1981.

[49] I. Lindgren and J. Morrison. *Atomic Many-Body Theory, 2nd Edition.* Springer-Verlag, 1986.

[50] J. Hata, I. P. Grant, and B. P. Das. *J. Phys.*, B16:L189, 1983.

[51] K. K. Baeck and Yoon Sup Lee. *J. Chem. Phys.*, 93:5775, 1990.

[52] S. R. Langhoff and C. W. Kern. In H. F. Shaefer III, editor, *"Modern Theoretical Chemistry Vol. 4, Applications of Electronic Structure Theory"*. Plenum Press, 1977.

[53] K. S. Pitzer. *Acc. Chem. Res.*, 12:271, 1979.

[54] P. Pyykko and J. P. Desclaux. *Acc. Chem. Res.*, 12:276, 1979.

[55] G. B. Bachelet, D. R. Hamann, and M. Schluter. *Phys. Rev.*, B26:4199, 1982.

[56] J. S. Cohen, W. R. Wadt, and P. Jeffrey Hay. *J. Chem. Phys.*, 71:2955, 1979.

[57] S. Koseki, M. W. Schmidt, and M. S. Gordon. *J. Phys. Chem.*, 96:10768, 1992.

[58] W. R. Wadt. *Chem. Phys. Lett.*, 89:245, 1982.

[59] S. Itoh, R. Saito, T. Kimura, and S. Yabushita. *J. Phys. Soc. of Jpn.*, 62:2924, 1993.

[60] J. C. Slater, T. M. Wilson, and J. H. Wood. *Phy. Rev.*, 179:29, 1969.

[61] S. Watanabe and H. Kamimura. *Mater. Sci. Eng.; J. Phys. Soc. Jpn; J. Phys.*, B3; 56; C 20:313; 1078; 4145, 1989; 1987; 1987.

[62] S. Huzinaga. *Gaussian Basis Sets for Molecular Calculations.* Elsevier, 1984.

[63] S. Huzinaga. *Bunshi kidou hou.* Iwanami, 1980.

[64] R. McWeeny. *Methods of Molecular Quantum Mechanics.* Academic, London, 1989. 2nd ed.

[65] In R. M. Pitzer, editor, *The Ohio State University, T.C.G. Report No. 101.* O.S.U., unpublished.

[66] C. F. Jackels and E. R. Davidson. *Int. Jour. Quant. Chem.*, 8:707, 1974.

[67] E. U. Condon and G. H. Shortley. *The Theory of Atomic Spectra.* Cambridge University Press, 1951.

[68] G. L. Malli. *Phys. Rev.*, A135:978, 1964.

[69] J. P. Desclaux. *Atomic Data and Nuclear Data Tables, Vol 12, 311-406.* Elsevier, 1976.

[70] S. Sugano, Y. Tanabe, and H. Kamimura. *Multiplets of Transition-Metal Ions in Crystal.* Academic, New York, 1970.

[71] G. H. Dieke and R. Sarup. *J. Chem. Phys.*, 29:741, 1958.

[72] J. Sugar. *Phys. Rev. Lett.*, 14:731, 1965.

[73] J. G. Conway and J. B. Gruber. *J. Chem. Phys.*, 32:1586, 1960.

[74] W. T. Carnall, H. Crosswhite, H. M. Crosswhite, and J. G. Conway. *J. Chem. Phys.*, 64:3582, 1976.

[75] L. G. DeShazer and G. H. Dieke. *J. Chem. Phys.*, 38:2190, 1963.

[76] K. S. Thomas ans S. Singh and G. H. Dieke. *J. Chem. Phys.*, 38:2180, 1963.

[77] M. H. Crozier and W. A. Runciman. *J. Chem. Phys.*, 35:1392, 1961.

[78] J. B. Gruber and J. G. Conway. *J. Chem. Phys.*, 32:1178, 1960.

Appendix

Gaussian Basis sets for rare earth atoms obtained by S. Huzinaga. This appendix is taken from the "Handbook of Gaussian Basis Sets for Molecular Calculations" by S. Huzinaga, (Elsevier, 1984) *pp.* 92 $\sim$ 93, 305 $\sim$ 341.

The table for Gaussian basis sets for phosphorus and rare earth atoms consists of (in atomic unit)

1. element (ground state for neutral atom), configuration, contraction patterns.
2. total energy (TE), potential energy (PE), kinetic energy (KE).
3. one-electron orbital energy (ORB E).
4. expectation values ($\langle r^n \rangle$) and the position of the maximum amplitude of the radial function ($r_{\max}$).
5. expansion coefficient (c) for obtaining the radial function for subshell by linear combination of appropriate basis functions.
6. exponent (e) of the Gaussian basis set.
7. contraction coefficient (d) of the contracted Gaussian basis sets.

It is useful for the future calculation to show the basis sets that we used in the present calculation. All basis sets are for neutral atom. In future, the optimization of the basis sets trivalent ions with relativistic effect should be taken intensively.

Since there are some contraction patterns for a atom, the contraction sets that we used in this thesis are specified by the symbol * at the atomic characters.